Nordisk kernesikkerhedsforskning
Norrænar kjarnöryggisrannsóknir
Pohjoismainen ydinturvallisuustutkimus
Nordisk kjernesikkerhetsforskning
Nordisk kärnsäkerhetsforskning
Nordic nuclear safety research

NKS-236
ISBN 978-87-7893-308-9

CFD and FEM modeling of PPOOLEX experiments

Timo Pättikangas, Jarto Niemi and Antti Timperi

VTT Technical Research Centre of Finland

January 2011

Abstract

Large-break LOCA experiment performed with the PPOOLEX experimental facility is analysed with CFD calculations. Simulation of the first 100 seconds of the experiment is performed by using the Euler-Euler two-phase model of FLUENT 6.3. In wall condensation, the condensing water forms a film layer on the wall surface, which is modelled by mass transfer from the gas phase to the liquid water phase in the near-wall grid cell. The direct-contact condensation in the wetwell is modelled with simple correlations. The wall condensation and direct-contact condensation models are implemented with user-defined functions in FLUENT.

Fluid-Structure Interaction (FSI) calculations of the PPOOLEX experiments and of a realistic BWR containment are also presented. Two-way coupled FSI calculations of the experiments have been numerically unstable with explicit coupling. A linear perturbation method is therefore used for preventing the numerical instability. The method is first validated against numerical data and against the PPOOLEX experiments. Preliminary FSI calculations are then performed for a realistic BWR containment by modeling a sector of the containment and one blowdown pipe. For the BWR containment, one- and two-way coupled calculations as well as calculations with LPM are carried out.

Key words

Large-break LOCA, Condensation pool, pressure suppression pool, BWR, CFD, fluid-structure interactions, FSI

NKS-236
ISBN 978-87-7893-308-9

Electronic report, January 2011

NKS Secretariat
NKS-776
P.O. Box 49
DK - 4000 Roskilde, Denmark

Phone +45 4677 4045
Fax +45 4677 4046
www.nks.org
e-mail nks@nks.org

RESEARCH REPORT

VTT-R-02187-10

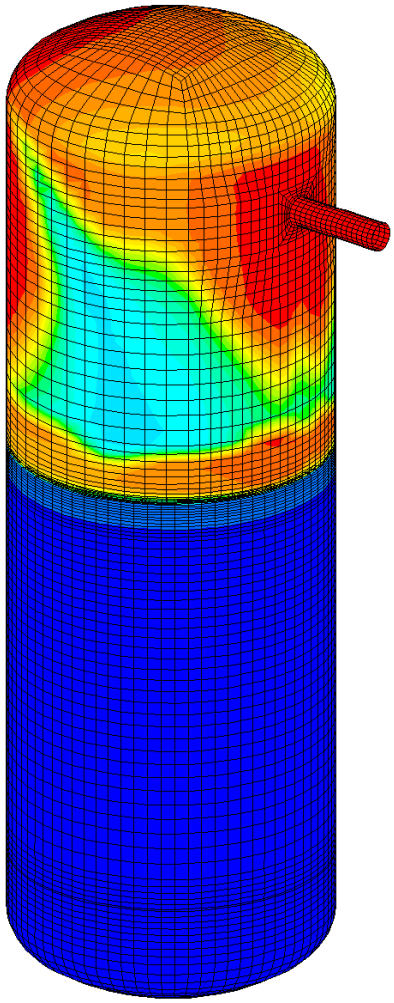

CFD and FEM modeling of PPOOLEX experiments

Authors: Timo Pättikangas, Jarto Niemi and Antti Timperi

Confidentiality: Public

Report's title	
CFD and FEM modeling of PPOOLEX experiments	
Customer, contact person, address	Order reference
1. Valtion ydinjäterahasto, Työ- ja elinkeinoministeriö, PL 32, 00023 VALTIONEUVOSTO 2. Nordic nuclear safety research (NKS), Vattenfall Power Consultant AB, Patrick Isaksson, Box 527, SE-162 16 Stockholm, Sweden	1. SAFIR2010 Programme: ad 9/2007SAF 2. NKS Contract no. AFT/NKS-R(09)58/9
Project name	Project number/Short name
Numerical modeling of condensation pool	32109 / NUMPOOL2009
Author(s)	Pages
Timo Pättikangas, Jarto Niemi and Antti Timperi	39
Keywords	Report identification code
Condensation pool, pressure suppression pool, BWR, CFD, fluid-structure interactions, FSI	VTT-R-02187-10

Summary

Computational fluid dynamics simulation of the first 100 seconds of the experiment is performed by using the Euler-Euler two-phase model of FLUENT 6.3. In the model, the gas phase consists of air and vapour species components. In wall condensation, the condensing water forms a film layer on the wall surface, which is modelled by mass transfer from the gas phase to the liquid water phase in the near-wall grid cell. The heat transfer from the gas phase through the water film to the wall is resolved. The direct-contact condensation in the wetwell is modelled with simple correlations. The wall condensation and direct-contact condensation models are implemented with user-defined functions in FLUENT.

Fluid-Structure Interaction (FSI) calculations of the PPOOLEX experiments and of a realistic BWR containment are also presented. In the FSI calculations, the motion of the structures is taken into account when the pressure loads on the structures are calculated. Star-CD is used for CFD calculations and Abaqus for structural analysis. The external MpCCI code is used for coupling the CFD and structural analysis codes. Two-way coupled FSI calculations of the experiments have been numerically unstable with explicit coupling. A linear perturbation method is therefore used for preventing the numerical instability. The method is first validated against numerical data and against the PPOOLEX experiments. Preliminary FSI calculations are then performed for a realistic BWR containment by modeling a sector of the containment and one blowdown pipe. For the BWR containment, one- and two-way coupled calculations as well as calculations with LPM are carried out.

Confidentiality	Public

Espoo, 30.4.2010

Written by	Reviewed by	Accepted by
Timo Pättikangas, Senior Research Scientist	Mikko Manninen, Team Manager	Timo Vanttola Technology Manager

VTT's contact address
VTT, P.O.B. 1000, FI-02044 VTT, Finland

Distribution (customer and VTT)
Patrick Isaksson (NKS), STUK, Timo Toppila (FNS), Vesa Suolanen (VTT), Pavel Kudinov (KTH), Vesa Tanskanen (LUT), Markku Puustinen (LUT), Heikki Purhonen (LUT), Jani Laine (LUT), SAFIR2010 Reference Group 4

The use of the name of the VTT Technical Research Centre of Finland (VTT) in advertising or publication in part of this report is only permissible with written authorisation from the VTT Technical Research Centre of Finland.

Contents

Nomenclature 3

1 Introduction.....4

2 PPOOLEX experimental facility 5

3 CFD model for condensation 6

3.1 Wall condensation.....6
3.2 Direct contact condensation.....8

4 CFD modelling of the experiment WLL-05-02.....10

5 Fluid-structure interaction calculations 20

5.1 Order-of-magnitude analysis.....20
5.2 Comparison with two-way coupling.....22
5.3 Comparison with PPOOLEX experiment.....23
5.4 Modeling of realistic BWR containment 26

6 Summary and conclusions.....38

References 39

Nomenclature

Latin letters

c	speed of sound
C_p	specific heat capacity (J/kg)
g	acceleration of gravity
$\mathbf{g}$	acceleration of gravity vector
h	enthalpy (J/kg)
htc	heat transfer coefficient (W/m^{2}K)
L	length
$\dot{m}''$	mass flux density (kg/m^{2}s)
p	pressure
Q''	heat flux density (W/m^2)
t	time
T	temperature
$\mathbf{T}$	viscous stress tensor
V	velocity
$\mathbf{V}$	velocity vector
w	wall displacement
w	molecular weight
y	mole fraction
Y	mass fraction

Greek letters

μ	molecular viscosity
ρ	density

Subscripts

air	air species component of the gas phase
i	interface
gas	gas phase in the Euler-Euler model
sat	saturated state
steam	vapour species component of the gas phase
tot	total
water	liquid phase in the Euler-Euler model

1 Introduction

In boiling water reactors (BWR), the major function of the containment system is to protect the environment if a loss-of-coolant accident (LOCA) should occur. The containment is designed to accommodate the loads generated in hypothetical accidents, such as sudden rupture of a main steam line. In such an accident, a large amount of steam is suddenly released in the containment. An essential part of the pressure suppression containment is a water pool, where condensation of released steam occurs.

In a BWR, the pressure suppression containment typically consists of a drywell and a wetwell with a water pool. In a hypothetical LOCA, steam and air flow from the drywell through a vent pipe to the wetwell, where the outlet of the vent pipe is submerged in the water pool. In early part of the accident, mainly non-condensable air or nitrogen flows through the vent pipe into the wetwell. Then, the volume fraction of vapour increases in the gas mixture. When all the non-condensable gas from the drywell is blown into the wetwell, the blowdown consists of pure vapour. The pressure suppression pool changes this large volume of vapour to a small volume of water (Lahey and Moody, 1993).

PPOOLEX test facility is a scaled-down model of a pressure suppression containment of a BWR (Laine and Puustinen, 2009). The pressurized PPOOLEX vessel shown in Figure 1 consists of a drywell compartment and a wetwell compartment with a water pool. The compartments are connected with a vent pipe, whose outlet is submerged in water pool in the wetwell. In experiments, vapour is generated in a steam generator and blown into the drywell.

In the PPOOLEX experiment WLL-05-02, vapour was blown into the preheated drywell compartment of the facility. The vapour jet hit the opposite wall of the drywell, where wall condensation occurred. The temperature of the wall structures of the dry well rose and heat was conducted through uninsulated walls to the ambient laboratory. When the pressure in the drywell increased, the mixture of air and vapour started flowing through the vent pipe into the water pool of the wetwell. The vent pipe was cleared of water and large gas bubbles formed at the pipe outlet with a frequency of about one hertz. The volume fraction of vapour in the drywell increased and direct-contact condensation at the outlet of the vent pipe became significant.

In the present work, a computational fluid dynamics (CFD) simulation of the first 100 seconds of the experiment is performed by using the Euler-Euler two-phase model of FLUENT 6.3. In the model, the gas phase consists of air and vapour species components. In wall condensation, the condensing water forms a film layer on the wall surface, which is modelled by mass transfer from the gas phase to the liquid water phase in the near-wall grid cell. The heat transfer from the gas phase through the water film to the wall is resolved. The direct-contact condensation in the wetwell is modelled with simple correlations. The wall condensation and direct-contact condensation models are implemented with user-defined functions in FLUENT.

Fluid-Structure Interaction (FSI) calculations of the PPOOLEX experiments and of a realistic BWR containment are also presented. In the FSI calculations, the motion of the structures is taken into account when the pressure loads on the structures are calculated. Star-CD is used for CFD calculations and Abaqus for structural analysis. The external MpCCI code is used for coupling the CFD and structural analysis codes. Two-way coupled FSI calculations of the experiments have been numerically unstable with explicit coupling. A linear perturbation

method (LPM) (Huber et al., 1979; Sonin, 1980; Timperi, 2009) is therefore used for preventing the numerical instability. The method is first validated against numerical data and against the PPOOLEX experiments. Preliminary FSI calculations are then performed for a realistic BWR containment by modelling a sector of the containment and one blowdown pipe. For the BWR containment, one- and two-way coupled calculations as well as calculations with LPM are carried out.

In Section 2, the PPOOLEX facility and the experiment WLL-05-02 are described. The two-phase CFD models for condensation are described in Section 3. In Section 4, the CFD results for the experiment WLL-05-02 are presented and compared to the measurements. In Section 5, the FSI calculations are presented the LPM method is described. The results obtained with the LPM method are compared to results obtained with full two-way coupling of the CFD and FEM codes. First results on modelling a realistic BWR containment are presented. Finally, Section 6 contains summary and discussion.

2 PPOOLEX experimental facility

PPOOLEX is an about 31 m^3 pressurized cylindrical vessel with a height of 7.45 meters and a diameter of 2.4 meters. The volume of the drywell compartment is 13.3 m^3 and the volume of the wetwell compartment is 17.8 m^3. The DN200 (∅219.1 × 2.5 mm) vent pipe is positioned in a non-axisymmetric location 300 mm away from the centre of the facility. The water level in the beginning of the experiments was 2.14 m from the bottom of the pool. The submergence depth of the DN200 vent pipe was 1.05 m, which corresponds to a hydrostatic pressure of about 10.2 kPa at the vent pipe outlet. The PPOOLEX facility is shown in Figure 1.

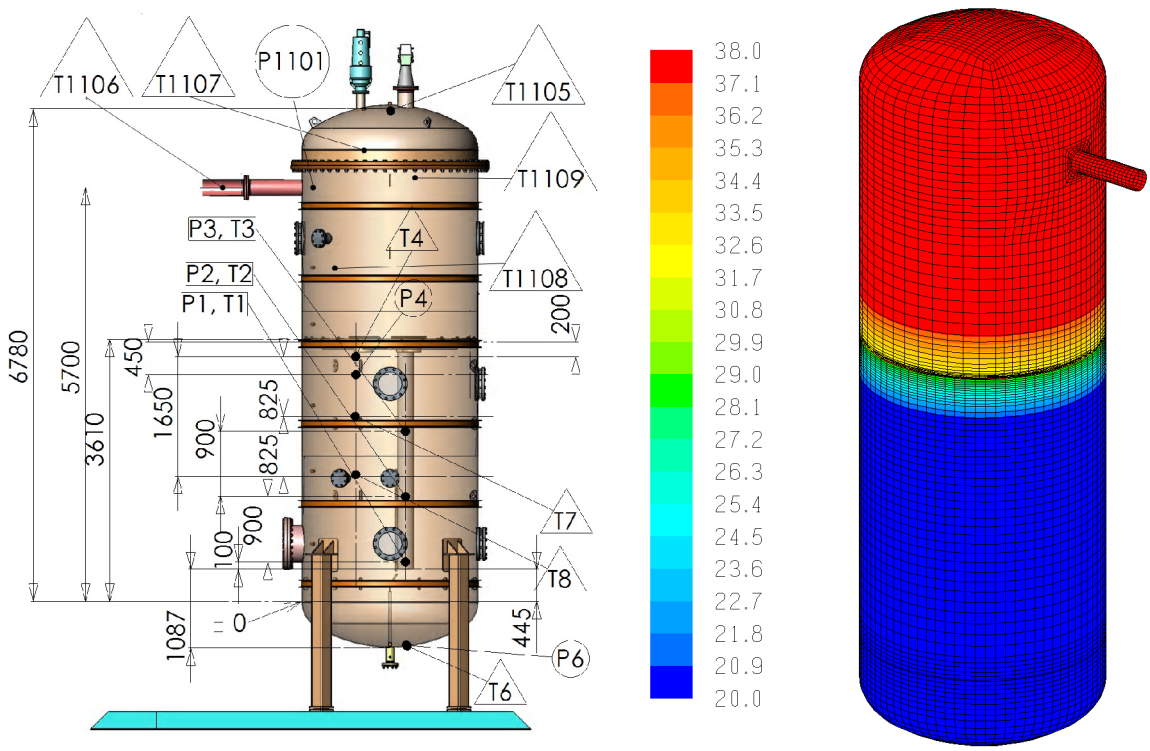

Figure 1. Pressure (Pn) and temperature (Tn) measurements in the PPOOLEX pressurized test facility at Lappeenranta University of Technology (Laine and Puustinen, 2008). On the right, the surface mesh and the outer wall temperature (C) at time t = 0 are shown.

In the experiments, pure vapour was blown into the drywell compartment of the PPOOLEX facility through the horizontal DN200 pipe. Vapour was obtained from the PACTEL steam generator connected to the DN200 pipe with a DN50 pipe. The mass flow rate of vapour into the drywell was measured with a vortex meter located in the DN50 line. In addition, the temperature of vapour was measured in the inlet plenum. The measured mass flow rate and temperature were used as boundary conditions in the CFD simulations.

Three different condensation phenomena occur in the experiments. First, some bulk condensation of vapour may occur, when vapour flows from the DN50 pipe through the DN200 inlet plenum into the drywell. Second, part of the vapour is condensed on the walls of the drywell. The wall condensation is determined by the initial wall temperature in the drywell and by the heat transfer through the walls of the drywell to the laboratory. Third, direct-contact condensation occurs in the water pool of the wetwell, when vapour flows from the drywell to the wetwell.

3 CFD model for condensation

The Euler-Euler model of FLUENT 6.3 was used in modelling the experiment. In the Euler-Euler model, the conservation equations of mass, momentum and enthalpy are solved for the gas phase and liquid phase. The gas phase is wet air, which consists of two species components: dry air and vapour. Transport equation is solved for the mass fraction of air Y_{air} in the gas phase and the mass fraction of vapour is $Y_{\mathrm{steam}} = 1 - Y_{\mathrm{air}}$. Gas phase is treated as a compressible ideal gas, where wall condensation, direct-contact condensation and bulk condensation are modelled with user-defined functions of FLUENT.

3.1 Wall condensation

The idea of the diffusive wall condensation model is illustrated in Fig. 2, where the mass and energy balances at the gas-liquid interface are shown. In condensation or evaporation, the mass balance reads

$$\dot{m}''_{\mathrm{steam}} = \dot{m}''_{\mathrm{water}} \tag{1}$$

where $\dot{m}''_{\mathrm{steam}}$ is the mass sink or source in the gas phase and $\dot{m}''_{\mathrm{water}}$ is the mass source or sink in the liquid phase. The energy balance at the interface is

$$Q''_{\mathrm{gas}} + \dot{m}''_{\mathrm{steam}} h_{\mathrm{steam}}(T_{\mathrm{steam}}) = Q''_{\mathrm{liquid}} + \dot{m}''_{\mathrm{water}} h_{\mathrm{water}}(T_{\mathrm{water}}) \tag{2}$$

where T_{steam} and T_{water} depend on the direction of the mass transfer (i.e., condensation or evaporation)

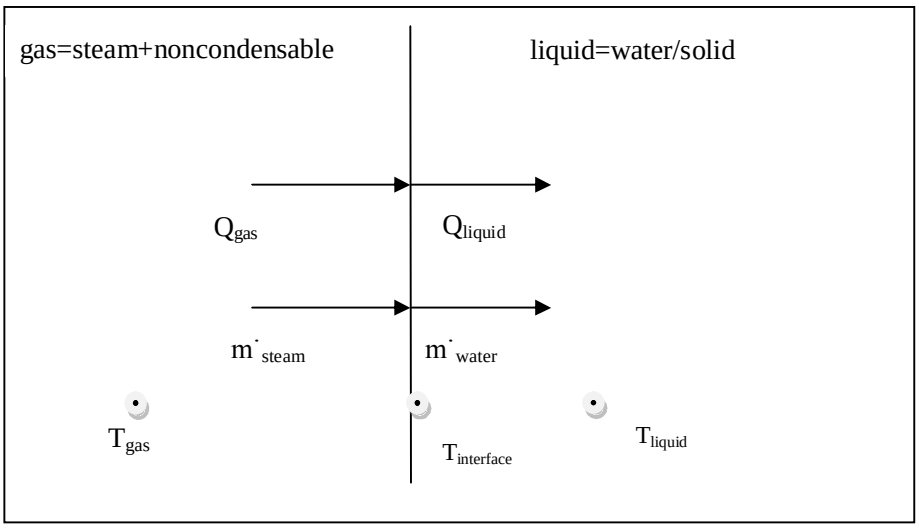

Figure 2. Heat transfer from the gas phase through the liquid film to the solid wall.

In condensation, steam disappears at the gas temperature T_{gas} and water appears at the interface temperature T_{i} . In evaporation, steam appears at the interface temperature T_{i} and water disappears at the liquid temperature T_{liquid}. The enthalpies are estimated by

$$h_{\text{water}}(T) = h_{\text{water}}(T_{\text{i}}) + C_{p,\text{water}}(T - T_{\text{i}})$$
$$h_{\text{steam}}(T) = h_{\text{steam}}(T_{\text{i}}) + C_{p,\text{steam}}(T - T_{\text{i}}) \tag{3}$$

The heat fluxes are determined by

$$Q''_{\text{gas}} = htc_{\text{gas}}(T_{\text{gas}} - T_{\text{i}})$$
$$Q''_{\text{liquid}} = htc_{\text{liquid}}(T_{\text{i}} - T_{\text{liquid}}) \tag{4}$$

The condensation mass flux is determined by diffusion model

$$\dot{m}''_{\text{steam}} = -\frac{w_{\text{steam}}}{w_{\text{mixture}}} mtc \cdot \ln\left(\frac{1 - y_{\text{steam}}}{1 - y_{\text{i}}}\right) \tag{5}$$

where y_{steam} is the mole fractions of steam in the near-wall grid cell and y_{i} is the mole fraction of steam in the interface. The turbulent mass transfer coefficient is mtc and w_{steam} and w_{mixture} are the molecular weights of steam and mixture, respectively. The mole fraction of steam at the interface is a function of the interface temperature:

$$y_{\text{i}}(T_{\text{i}}) = p_{\text{sat}}(T_{\text{i}}) / p_{\text{tot}} \tag{6}$$

The interface temperature T_{i} is determined by using Eqs (3)–(6) so that Eq. (2) is satisfied.

3.2 Direct contact condensation

A simple model was used for describing the direct-contact condensation in the water pool. The model is intended to describe the basic features of direct-contact condensation in two-phase simulations with FLUENT. The idea of the model is illustrated in Fig. 3.

In the model, the properties of the phases (T_{gas}, y_{steam}, T_{liquid}) and the heat transfer coefficients (htc_{gas} , htc_{liquid} , htc_{solid}) are assumed to be known. The gas phase is treated as two component mixture, a condensable and a non-condensable gas component. The effects of the components to the heat transfer are estimated from the volume fractions of the components. That is, the heat transfer area is reduced by the mole fraction (y_{air}, y_{steam}) of the component.

Mass and heat transfer at the gas-liquid interface is determined by the phase properties (T_{gas}, T_{liquid}) of the fluid.

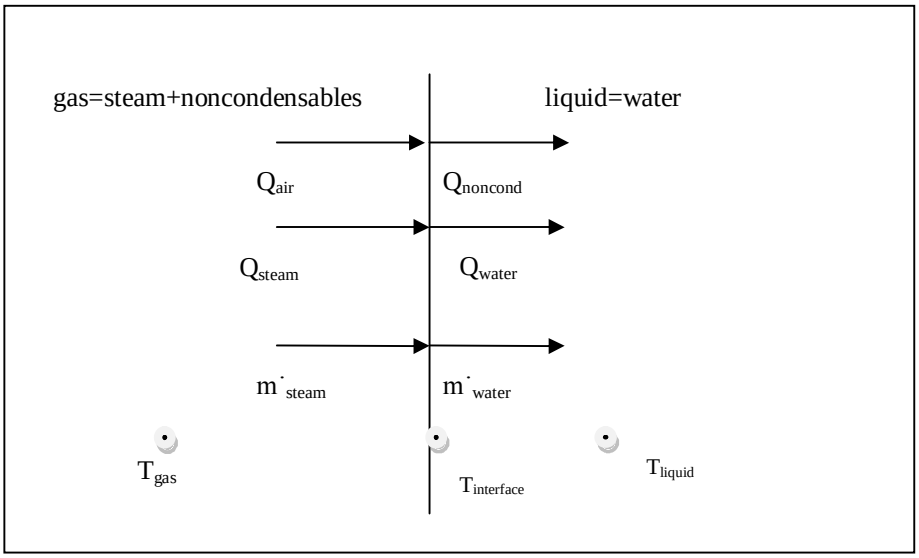

Figure 3. Interface energy balance of heat fluxes (Q) and mass fluxes ($\dot{m}$).

The mass balance at the interface is again given by Eq. (1). The energy balance at the interface

$$Q''_{air} + Q''_{steam} + \dot{m}''_{steam} h_{steam}(T_{steam}) = Q''_{noncond} + Q''_{water} + \dot{m}''_{water} h_{water}(T_{water}) \tag{7}$$

where T_{steam} and T_{water} depend on the direction of mass transfer. In condensation, steam disappears at the gas temperature T_{gas} and water appears at the saturation temperature T_{sat} . In evaporation, steam appears at the saturation temperature T_{sat} and water disappears at the liquid temperature T_{liquid}. The enthalpies are estimated by Eq. (3), where the interface temperature is $T_i = T_{sat}$.

The heat transfer of the non-condensable gas component is determined by

$$Q''_{air} = Q''_{noncond} = y_{air} \frac{htc_{gas} \cdot htc_{liquid}}{htc_{gas} + htc_{liquid}} \left(T_{gas} - T_{liquid}\right) \tag{8}$$

The condensation or evaporation is determined by the saturation temperature of the condensable gas component:

$$T_{\text{sat}} = T_{\text{sat}}(p_{\text{steam}}) \tag{9}$$

The heat fluxes are

$$Q''_{\text{steam}} = y_{\text{steam}} \cdot htc_{\text{gas}} \left(T_{\text{gas}} - T_{\text{sat}}\right) \tag{10}$$

$$Q''_{\text{water}} = y_{\text{steam}} \cdot htc_{\text{liquid}} \left(T_{\text{sat}} - T_{\text{liquid}}\right) \tag{11}$$

When condensation occurs, i.e., $Q''_{\text{water}} > Q''_{\text{steam}}$, the mass flux of steam is

$$\dot{m}''_{\text{steam}} = \frac{Q''_{\text{water}} - Q''_{\text{steam}}}{h_{\text{fg}} + C_{p,\text{gas}}\left(T_{\text{gas}} - T_{\text{sat}}\right)} \tag{12}$$

where the latent heat is $h_{\text{fg}} = h_{\text{steam}}(T_{\text{sat}}) - h_{\text{water}}\left(T_{\text{sat}}\right)$. When evaporation occurs, the mass flux of steam is

$$\dot{m}''_{\text{steam}} = \frac{Q''_{\text{water}} - Q''_{\text{steam}}}{h_{\text{fg}} - C_{p,\text{liquid}}\left(T_{\text{liquid}} - T_{\text{sat}}\right)} \tag{13}$$

In the FLUENT model, a volumetric mass transfer rate is needed, which is obtained by multiplying the mass flux by area density. The area density is estimated by $ai = |\nabla \alpha|$, where α is the void fraction.

In the present simulation, the heat transfer coefficient of gas has a constant value of htc_{gas} = 1000. The heat transfer coefficient for liquid is calculated from the correlation of Chen and Mayinger: $htc_{\text{liquid}} = 0.185\,\text{Re}^{0.7}\,\text{Pr}^{0.5}$.

4 CFD modelling of the experiment WLL-05-02

The CFD mesh of the PPOOLEX facility consists of 135 000 hexahedral grid cells. The surface mesh is shown in Fig. 1. The QUICK scheme was used for the spatial discretization of the volume fraction equation and the second order upwind scheme for other variables. The first order implicit method was used for the time discretization with a time step of Δt = 0.01 s. The gas phase was modelled as compressible ideal gas, and the floating operating pressure option of FLUENT was used.

In the PPOOLEX experiment WLL-05-02, vapour was blown into the preheated drywell compartment of the facility. The initial temperature of the drywell was about 65 °C, and the initial temperature of the water pool in the wetwell compartment was about 20 °C. The initial mole fraction of vapour in the gas phase was y_{steam} = 0.01. Temperature of the ambient laboratory was 25 °C. The heat transfer coefficient from the uninsulated wall to the ambient laboratory was assumed to be 4.53 W/m^{2}K, and the emissivity of the outer wall was assumed to be ε = 0.3. The thickness of the steel wall of the drywell was 8 mm.

In the experiment, a gas jet was injected into the drywell through the inlet plenum. In the CFD calculation, the gas was almost pure vapour containing a mass fraction of one percent of air. The maximum mass flow rate of the jet was 0.54 kg/s, and the vapour temperature in the inlet plenum was about 140 °C. The mass flow rate into the drywell is shown in Fig. 4.

When the pressure in the drywell increases, the water plug in the vent pipe starts moving downwards. The vent pipe is cleared at time t = 6 s and the first bubble is formed at the outlet of the vent pipe in the water pool. After this, new bubbles are formed with a period of about 0.72 s. The periodic formation of bubbles can be clearly seen in the mass flow rate through the vent pipe that is shown in Fig. 4. When bubbles are detached from the vent outlet, the mass flow rate in the vent pipe becomes for awhile almost zero or is even reversed.

In Fig. 5, the temperature of the gas phase is shown at a few instants of time. The initial temperature of the preheated drywell is somewhat stratified. Some heat conduction occurred through the floor of the drywell to the top part of the wetwell. The temperature was initialized to correspond to the measured temperatures at time t = 0. The initial temperature of the outer wall is shown in Fig. 1.

The hot steam jet injected into the drywell is seen in Fig. 5. The temperature of the drywell rises during the first 100 s to about 120 °C. The temperature of the outer wall at time t = 100 s is shown on the front cover of this report. The temperature scale is from 20 °C to 120 °C.

In Fig. 6, the mole fraction of vapour in the gas phase is shown. The mole fraction of vapour increases rapidly from its initial value of one percent. At time t = 100 s, the mole fraction of vapour is about 90% in the drywell. At this time, the gas flowing through the vent pipe into the water pool contains almost 80 % of vapour. Strong condensation of vapour occurs on the walls of the drywell and on the walls of the vent pipe that is submerged in cold water.

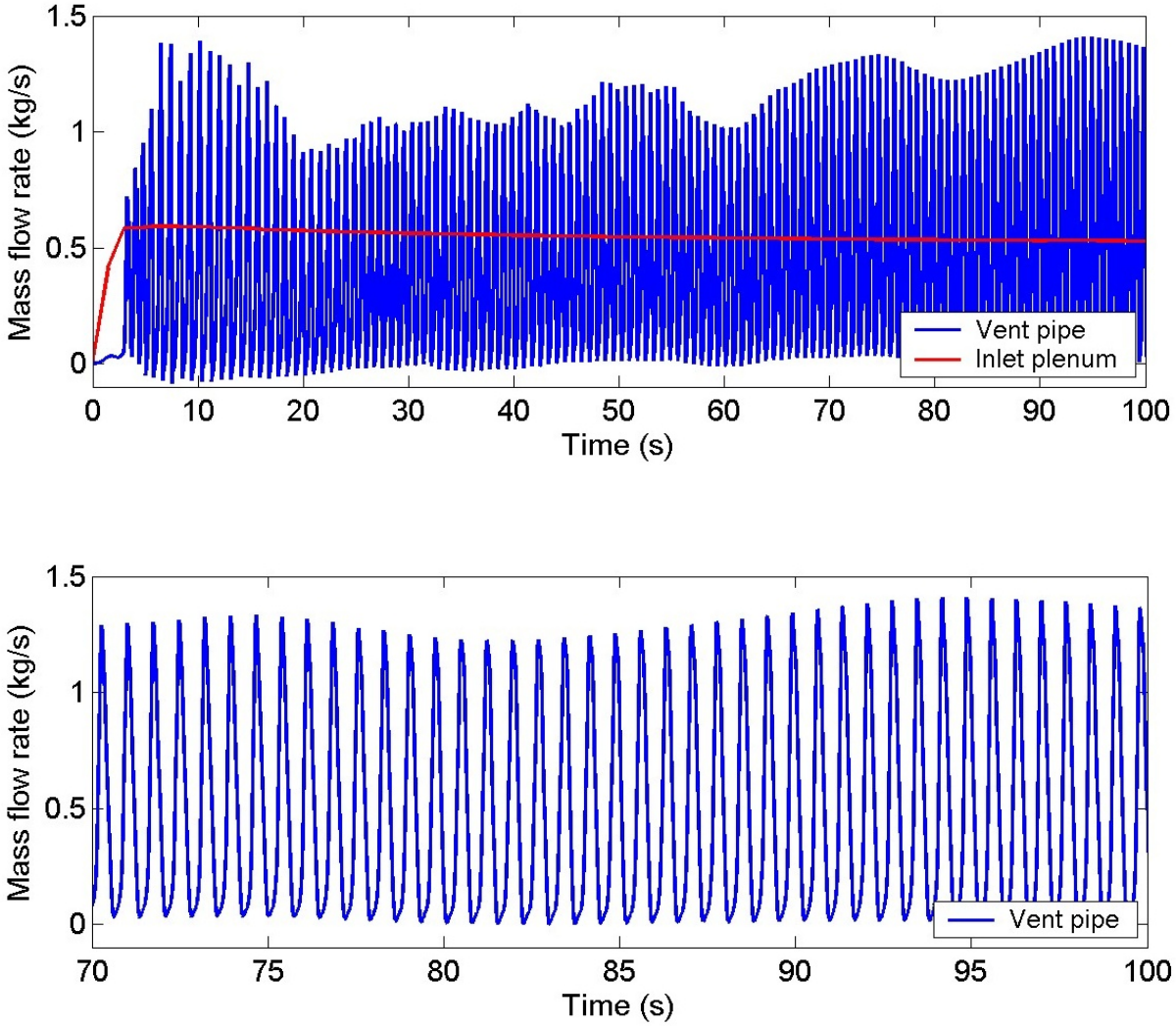

Figure 4. Mass flow rate (kg/s) into the drywell (red line) and through the vent pipe (blue line) versus time (s). Simulation of experiment WLL-05-02.

In Fig. 7, the wall condensation is shown on the wall of the drywell, where the injected vapour jet hits. In the beginning of the experiment, the wall is fairly cold. Therefore, condensation is first strong and decreases gradually. The maximum condensation rate is about 3.6 kg/m^{2}s, and it occurs at about t = 20 s.

In Fig. 8, the direct-contact condensation rate at the outlet of the vent pipe is illustrated at a few instants of time. In the early phase of the experiment, the gas flowing through the vent pipe contains mainly air and, therefore, almost no condensation occurs. Later in the experiment, when the gas in the vent pipe contains mainly vapour, strong condensation occurs near the outlet of the vent pipe. The condensation is, however, still affected by air, which has a mole fraction of about 20 %.

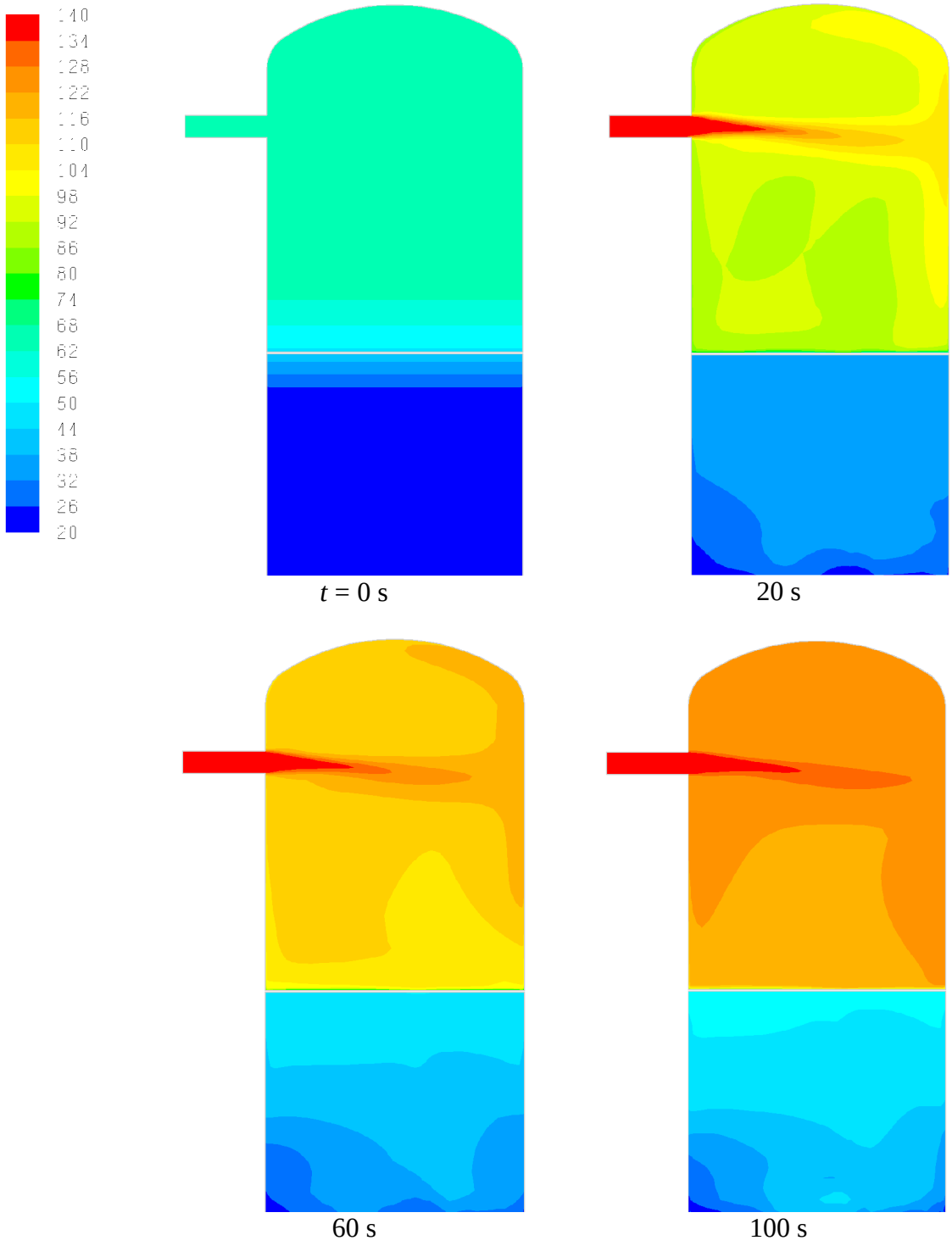

Figure 5. Temperature of gas (C) in the central cross-section at different instants of time.

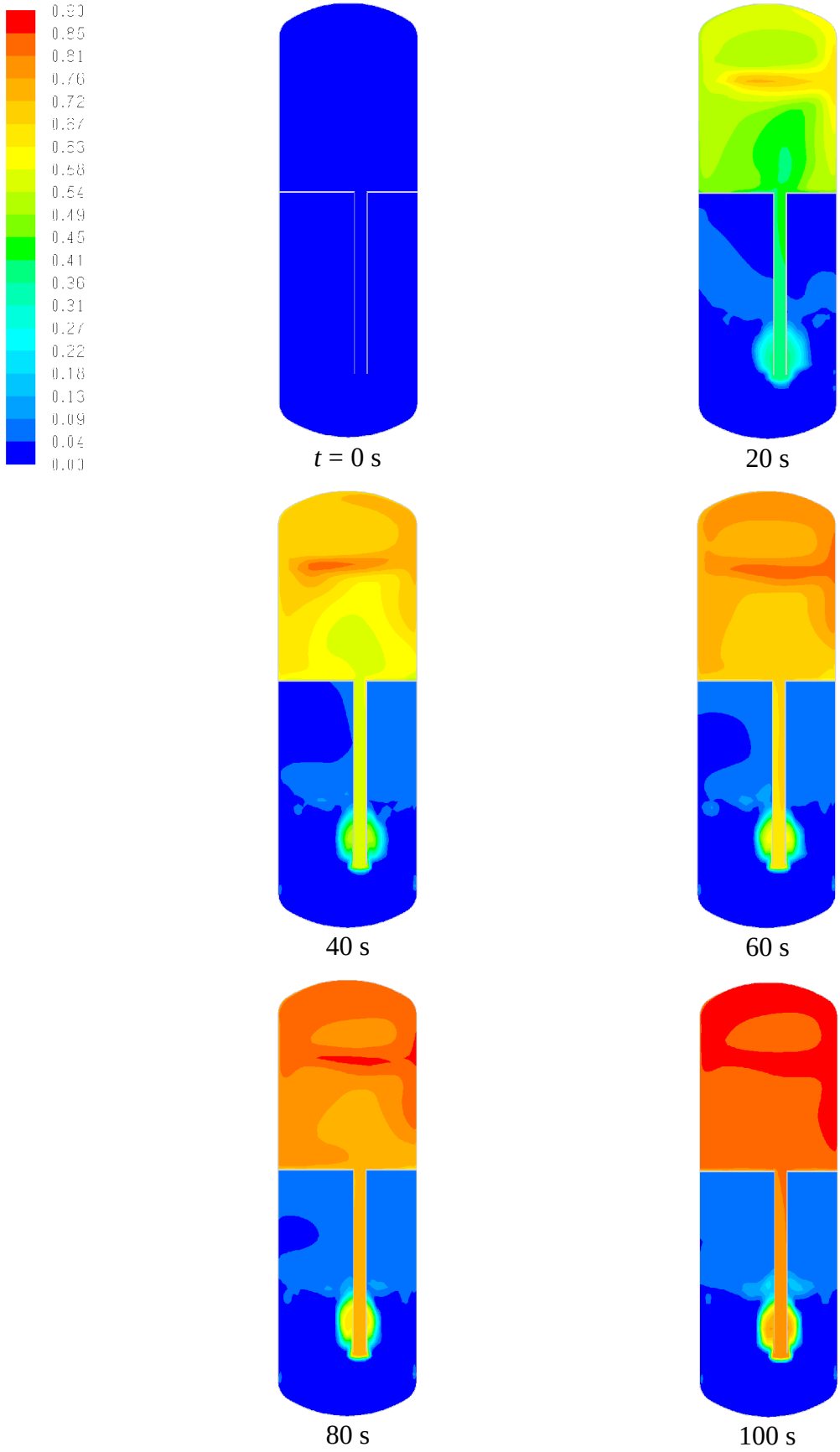

Figure 6. Mole fraction of vapour in the vent cross-section at different instants of time.

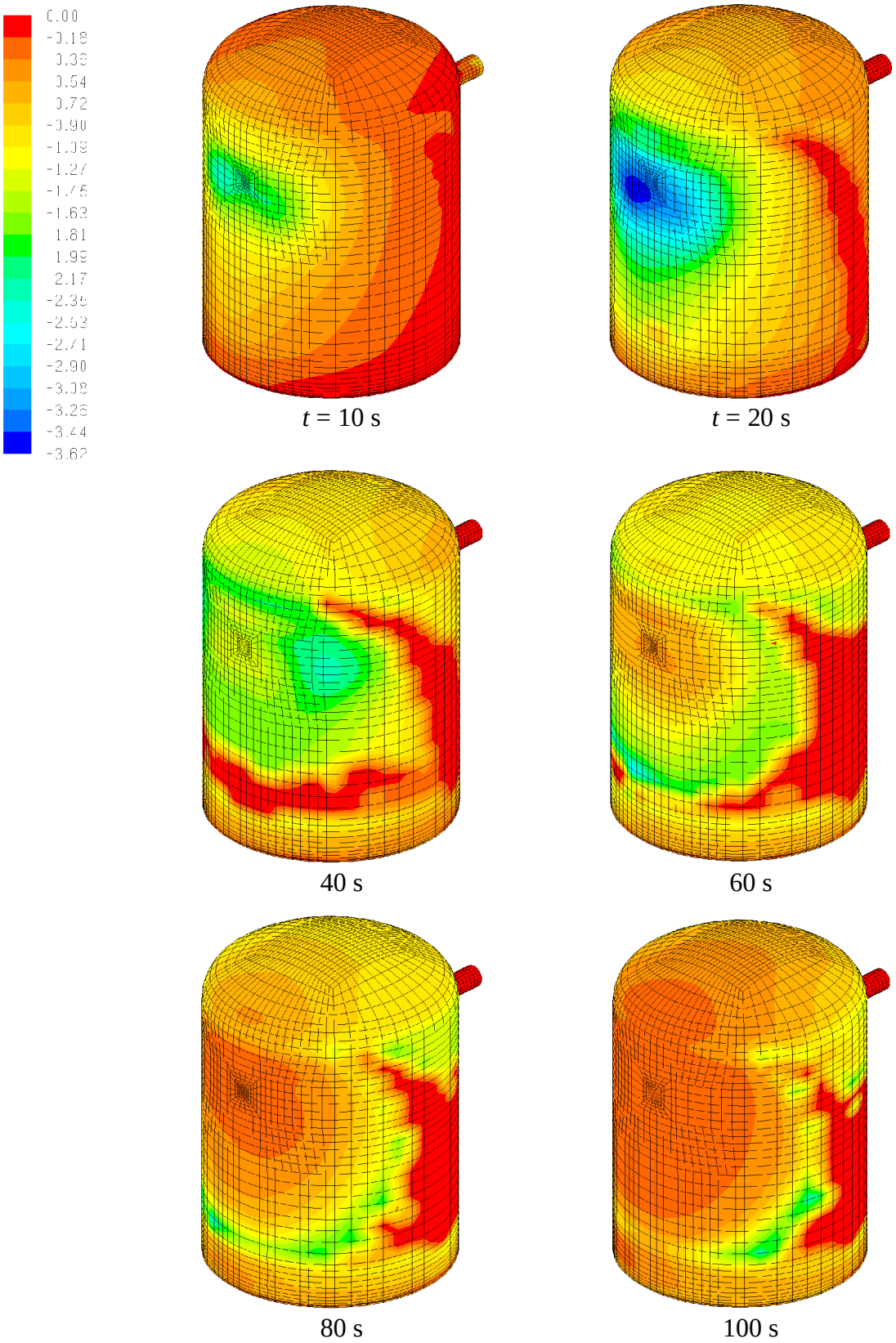

Figure 7. Mass transfer rate (kg/m^{2}s) between the gas and liquid phases in wall condensation.

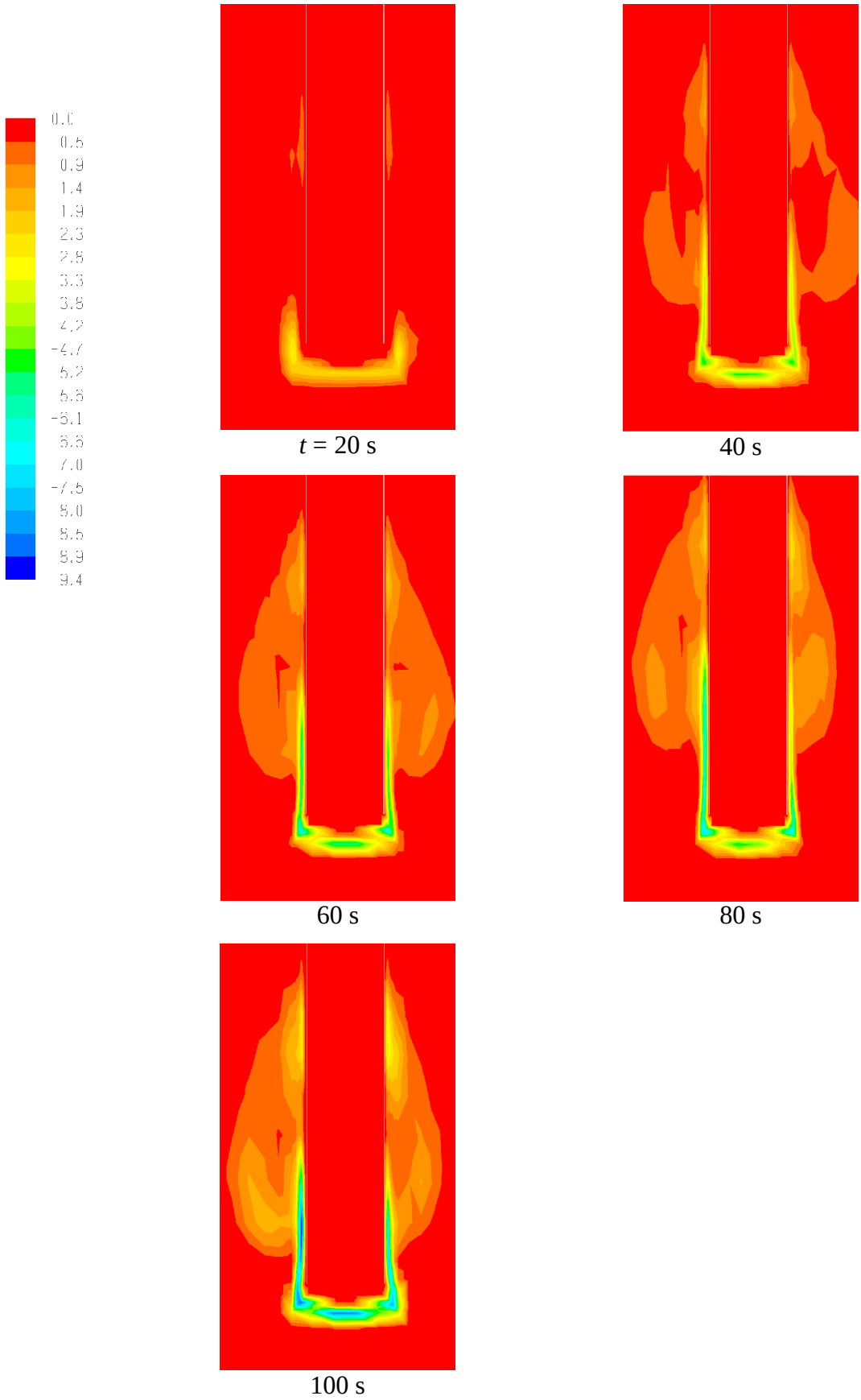

Figure 8. Mass transfer rate (kg/m^{3}s) between gas and liquid phase during direct-contact condensation at the outlet of the vent pipe.

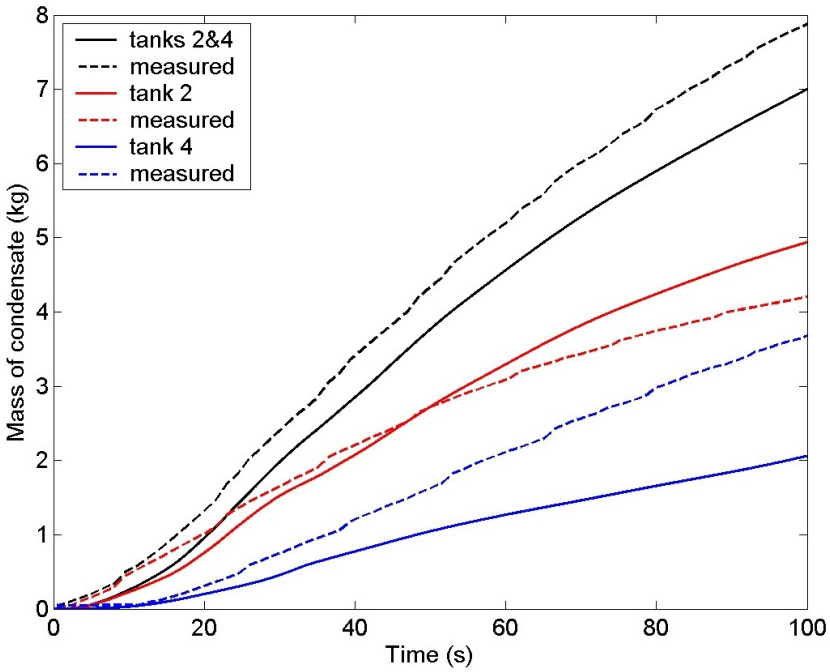

Figure 9. Cumulative mass of condensate in the lower gutter. A delay of 25 s caused by flow through gutter system is assumed in the calculated mass.

In the experiment, wall condensation in the drywell is studied by collecting condensate from the wall with a gutter system (Laine and Puustinen, 2009). The cumulative amount of condensate on the back wall, where the vapour jet hits first, is collected in tank 2 from a wall area of 5.25 m^2. The condensate from the front wall, where the inlet plenum is located, is collected in tank 4 from a wall area of 5.25 m^2. The flow of condensate through the gutter system to the tanks causes some delay in the experiment, which does not occur in the CFD calculation. Therefore, a delay of 25 s is estimated to occur in the experiment result.

The calculated results are compared to the measurements in Fig. 9, where the cumulative amount of condensate is shown. On the back wall, the condensation is slightly overestimated by the CFD calculation. On the front wall, the condensation is clearly underestimated by the calculation. In the total amount of condensation, the errors partly cancel each other. The calculated amount of condensation is about 10% smaller than the measurement.

The PPOOLEX facility was uninsulated when the experiment WLL-05-02 was performed. In the early phase of the experiment, the amount of wall condensation is determined by heat transfer from the gas to the solid structures of the facility. Later, the heat transfer from the outer wall to the ambient laboratory determines the amount of condensation. The heat transfer to the laboratory is only modelled with a heat transfer coefficient and an emissivity for radiation heat transfer. These parameters determine the accuracy of the present calculation.

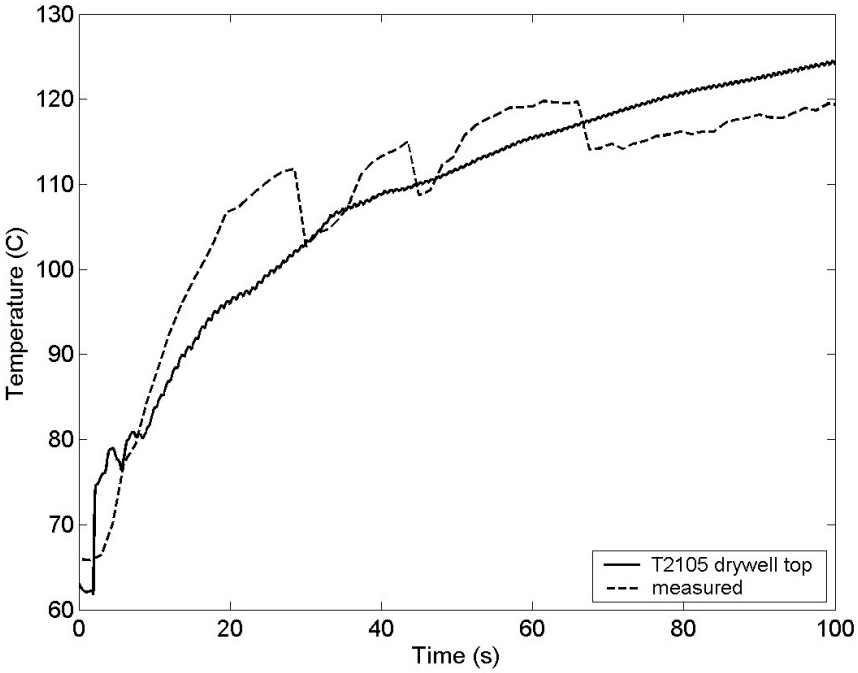

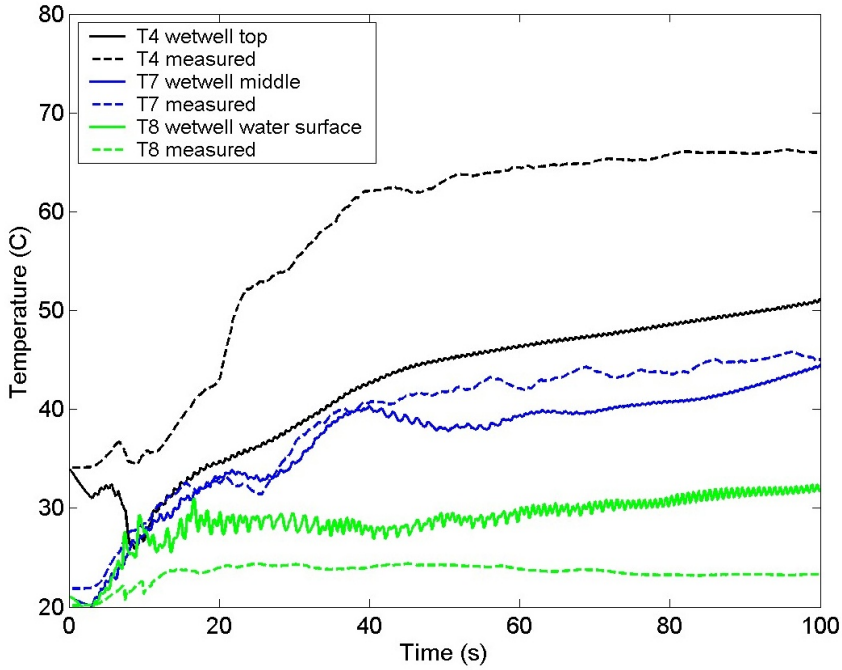

Figure 10. Comparison of the calculated and measured temperatures in the drywell (top) and in the wetwell (bottom).

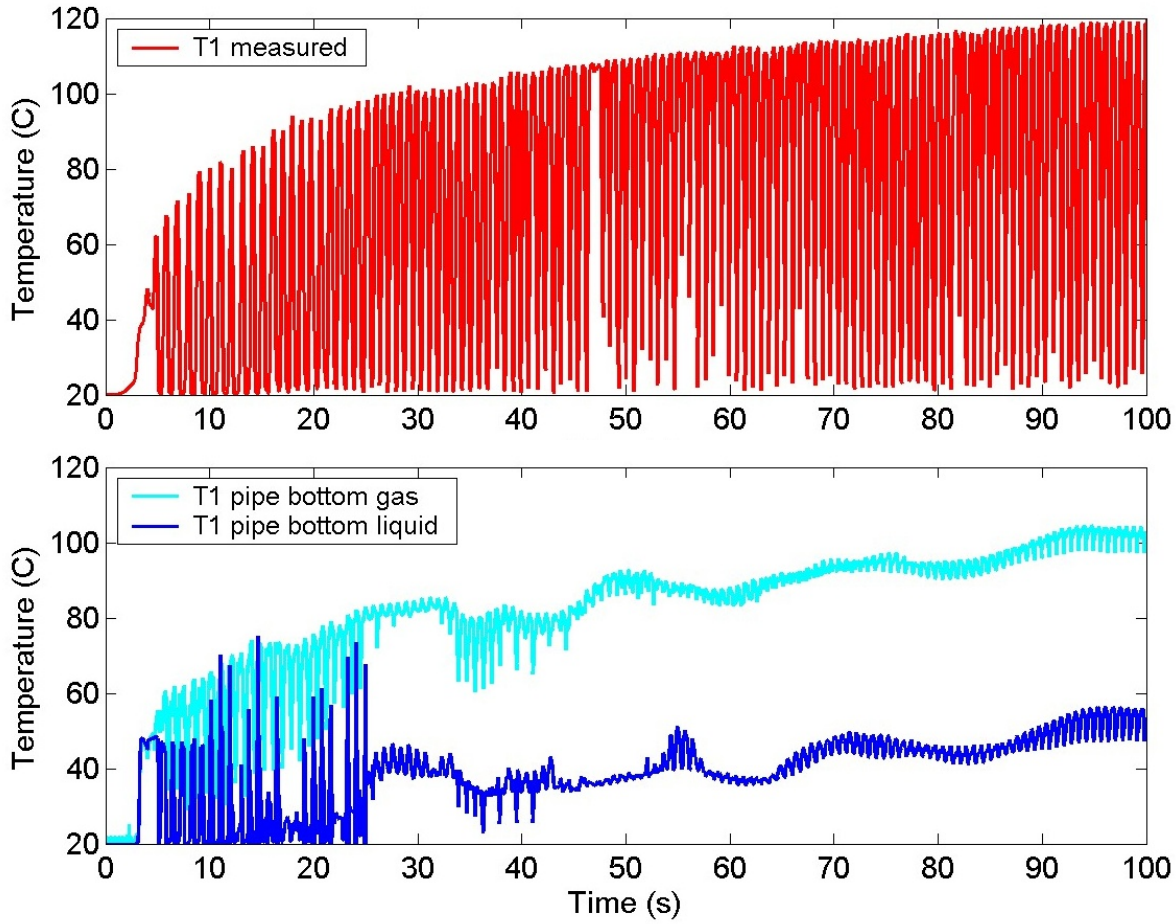

Figure 11. Measured temperature in the vent pipe (top) and the calculated temperatures of gas and liquid (bottom).

In Fig. 10, the calculated temperatures are compared to measurements at a few point in the drywell and in the wetwell. In the measured temperature, a few abrupt changes occur which are not captured by the calculation. Otherwise, the calculated temperature in the drywell is quite close to the measurement.

In the wetwell, the temperature is stratified already in the beginning of the experiment. The stratification partly is caused by the heat transferred through the drywell floor to the top part of the wetwell. The measurement shows that a stratified condition persists all the time during the experiment. In the calculation, however, more mixing occurs and stratification is weaker. The calculated temperature at the top of the wetwell drops already in the beginning of the calculation and differs from the measurement. The difference is at least partly caused by the turbulence modelling which was done with the standard k-ε model with wall functions for the mixture of the phases.

In Fig. 11, the measured temperature inside the vent pipe is shown. The measurement is done near the outlet of the pipe, where the sensor is initially submerged in water. When bubbles are forming at the outlet of the vent pipe, hot gas is surrounding the sensor. When the bubbles

detach from the vent outlet, water flows in the vent pipe surrounding the sensor. Therefore, the sensor alternates in measuring the gas and the water temperatures.

In the bottom part of Fig. 11, the calculated temperatures of gas and water are shown. The calculated temperatures of gas are somewhat lower than the measurements. The calculated temperature of water is higher than the measured value. This indicates that the calculated mixing of water near the vent outlet is not quite as strong as it is in reality.

The calculated pressures are compared to the measurements in Fig. 12. The calculated pressures are clearly higher than the measured values. The reason for this is the smaller amount of wall condensation in the drywell, which in turn is caused by too weak heat transfer to the ambient laboratory. In addition, the direct-contact condensation in the water pool is also too weak. In Fig. 6, one can see that some vapour is able to escape through the water pool to the gas space of the wet well. This is not expected to occur in reality. The reasons for this are the challenges in modelling the interfacial area and the heat transfer in the water pool.

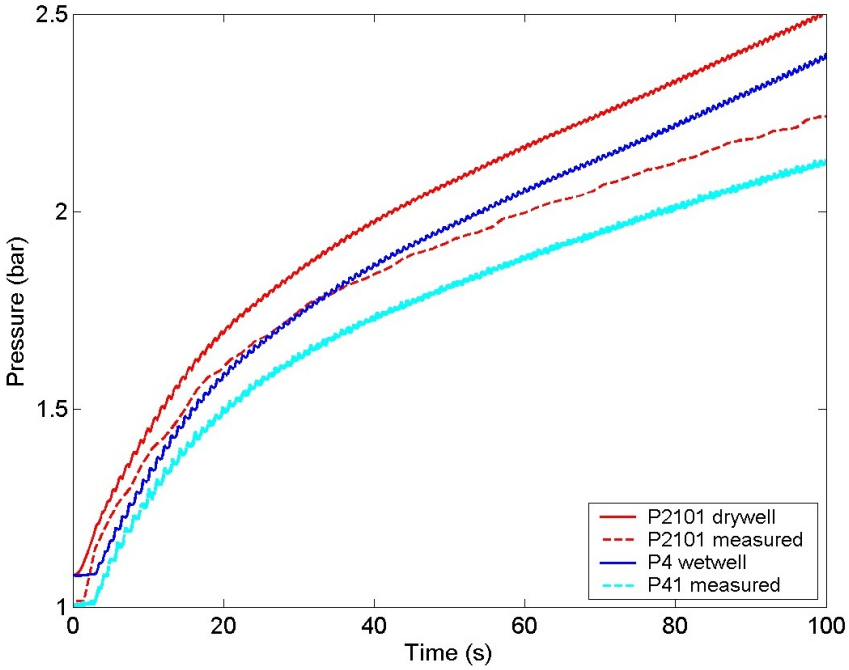

Figure 12. Comparison of the calculated pressure to measurement in the drywell and wetwell.

5 Fluid-structure interaction calculations

In this work, the linear perturbation method is used for circumventing the numerical instability which occurs with explicit two-way FSI coupling in some cases. Schematic of the method is presented in Fig. 13. The pressure load is transferred from the CFD model to the structural model, but no displacement feedback is sent back. The mass of the fluid is accounted for in the structural motion through a separate acoustic fluid which has two-way coupling with the structure. The method eliminates the numerical instability as the coupling between the CFD and structural models is only one-way and a stable monolithic approach is used for the acoustic-structural system (see e.g. Cook et al., 2002). In the method, two different flow fields are solved and superposed: flow field that would occur if the walls were rigid and flow field due to wall motion.

Mathematical analysis of the basis of the method and validation calculations are presented in Timperi (2009) and Pättikangas et al. (2009). In the following, the order-of-magnitude analysis of Timperi (2009) is first shortly reviewed by including also values for a realistic BWR containment. The method is then validated against numerical data and against the PPOOLEX experiment SLR-05-02. Preliminary FSI calculations of the blowdown in the realistic BWR containment are finally carried out. Stresses and effect of FSI in the BWR containment are studied.

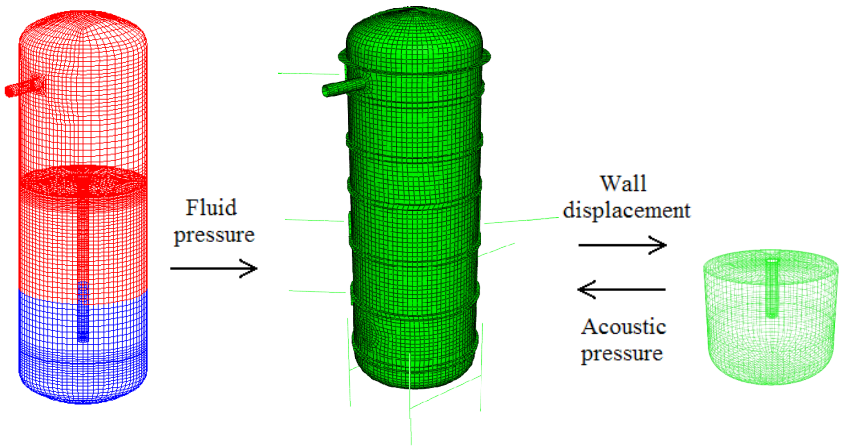

Figure 13. Schematic of the linear perturbation method and numerical models of the PPOOLEX facility. From left to right: CFD, structural and acoustic model.

5.1 Order-of-magnitude analysis

By starting from the conservation equations of mass and momentum for compressible fluid, the following dimensionless mass and momentum equations can be derived for the flow field due to pool wall motion (Timperi, 2009):

$$\Pi_1 \frac{\partial \rho_2 *}{\partial t *} + \rho_0 * \nabla * \cdot \mathbf{V}_2 * + \sqrt{\Pi_1 \Pi_3} (\rho_2 * \nabla * \cdot \mathbf{V}_1 * + \mathbf{V}_1 * \cdot \nabla * \rho_2 *) + \Pi_3 \mathbf{V}_2 * \cdot \nabla * \rho_1 * + \Pi_1 \Pi_4 \mathbf{V}_2 * \cdot \nabla * \rho_2 * = 0 \quad (14)$$

$$\rho_0 * \left(\frac{\partial \mathbf{V}_2 *}{\partial t *} + \Pi_2 ((\mathbf{V}_1 * \cdot \nabla *) \mathbf{V}_2 * + (\mathbf{V}_2 * \cdot \nabla *) \mathbf{V}_1 *) + \Pi_4 (\mathbf{V}_2 * \cdot \nabla *) \mathbf{V}_2 * \right) + \Pi_3 \rho_2 * \left(\frac{\partial \mathbf{V}_1 *}{\partial t *} + (\mathbf{V}_1 * \cdot \nabla *) \mathbf{V}_1 * \right) = -\nabla * p_2 * + \Pi_5 \nabla * \cdot \mathbf{T}_2 * + \Pi_6 \rho_2 * \mathbf{g} * \quad (15)$$

where the subscripts 1 and 2 stand for the rigid wall flow and flow due to wall flexure, respectively, and the dimensionless parameters are

$$\Pi_1 = \left(\frac{L}{c t_2^0} \right)^2 \quad \Pi_2 = \frac{t_2^0 V_1^0}{L} \quad \Pi_3 = \left(\frac{V_1^0}{c} \right)^2 \quad \Pi_4 = \frac{w}{L} \quad \Pi_5 = \frac{\mu t_2^0}{\rho L^2} \quad \Pi_6 = \frac{gL}{c^2} \quad (16)$$

The reference constants were chosen as follows:

L = characteristic length of the pool
w = maximum wall displacement
t_2^0 = periodic time of pool wall oscillation
V_1^0 = flow velocity in the pool
c = speed of sound in water
ρ = density of water
μ = viscosity of water
g = acceleration of gravity

If the values of the dimensionless parameters are small compared to unity, it indicates that we can to a good approximation simplify (14) and (15) to

$$\frac{\partial \rho_2}{\partial t} + \rho \nabla \cdot \mathbf{V}_2 = 0 \quad (17)$$

$$\rho \frac{\partial \mathbf{V}_2}{\partial t} = -\nabla p_2 \quad (18)$$

These can be combined with the linear equation of state $\Delta p / \Delta \rho = c^2$ to obtain the wave equation for p_2:

$$\frac{\partial^2 p_2}{\partial t^2} - c^2 \nabla^2 p_2 = 0 \quad (19)$$

which is solved in Abaqus in the acoustic-structural problem. The simplifications decouple the solutions of the flow with rigid walls and flow due to wall flexure. We may then solve the initial flow problem with rigid walls, transfer the transient wall pressure on the acoustic-structural problem and solve the acoustic-structural problem separately. After application of the transient wall pressure from flow solution 1, the motion of the walls drives the flow solution 2. A more detailed analysis can be found in Timperi (2009).

Tables 1 and 2 list estimates of the reference constants and the resulting values of the dimensionless parameters for the PPOOLEX facility and for the realistic BWR containment. Note that for the BWR containment, the wall displacement, the periodic time of wall motion and the flow velocity in the pool have been obtained from the calculations presented later in

Sec. 5.4, and the values should be considered as highly approximate. It is seen that the dimensionless parameters are small also for the BWR containment.

As shown later, also the two-way coupled calculation turned out to be stable for the BWR containment, at least with the used time step. Note also that the wall displacement for the BWR containment may become considerably larger for different loadings, e.g. for the condensation induced water hammer which has a rapid pressure pulse. On the other hand, the LPM is probably not required for this kind of a rapid pressure transient because a short time step stabilizes the two-way calculation.

Table 1. Values of the reference constants for the PPOOLEX and BWR pools.

Case	L [m]	w [m]	t_2^0 [s]	V_1^0 [m/s]	c [m/s]	ρ [kg/m^3]	μ [Pas]	g [m/s^2]
PPOOLEX	1	0.001	0.1	1	1000	1000	0.001	10
BWR	10	0.0001	0.05	10	1000	1000	0.001	10

Table 2. Values of the dimensionless parameters for the PPOOLEX and BWR pools.

Case	Π_1	Π_2	Π_3	Π_4	Π_5	Π_6
PPOOLEX	10^{-4}	10^{-1}	10^{-6}	10^{-3}	10^{-7}	10^{-5}
BWR	4×10^{-2}	5×10^{-2}	10^{-4}	10^{-5}	5×10^{-10}	10^{-4}

5.2 Comparison with two-way coupling

The method was first compared with a two-way coupled FSI calculation by using a simplified axisymmetric model of the PPOOLEX facility. The model had a rigid side wall and a bottom plate that experiences only vertical rigid-body motion. This kind of system resembles the real facility in that the most dominant mode is the vertical oscillation of the whole pool. Mass of the bottom plate was set to 700 kg which is considerably lighter than structures of the real facility; a light structure was chosen to have a more pronounced added mass effect. The spring stiffness and damping were set to 123 MN/m and 58 kNs/m, respectively. Eigenfrequencies of this system with and without the pool water are about 18 Hz and 67 Hz, respectively.

In the CFD calculation, the Volume Of Fluid (VOF) model was used for tracking the free surface and the k-ε model was used for modelling turbulence. Air was assumed incompressible and a logarithmic equation of state suitable for compressible liquid was used for water. A short time step of 40 µs, determined by stability of the two-way coupled calculation, was used in all calculations. Air velocity at the blowdown pipe inlet was ramped smoothly to a constant value of 30 m/s which is of the same order as in the experiments.

An explicit coupling scheme was used in the two-way FSI calculation. The flow field is solved by Star-CD and the fluid pressure is interpolated on the structure by MpCCI. The structural deformations and stresses are in turn solved by Abaqus and the wall displacement is interpolated on the CFD model. The surface nodes of the CFD model are moved accordingly and the internal mesh is smoothed to preserve the mesh quality. In the present simulation, the data exchange was performed once in each time step.

Fig. 14 shows the volume fraction of water in the pool at different instants of time. Pressures and displacements at the pool bottom are compared in Fig. 15. Results obtained with two-way coupling and with LPM are in good agreement whereas the one-way coupled calculation differs from these considerably. The clearly higher frequency of the wall motion in the one-way coupled case is due to the absence of the added mass effect. Note that maximum flow velocity is about 30 m/s near the pipe outlet but in these calculations validity of the method is unaffected by this (see Timperi, 2009). Furthermore, LPM works well in this case although the free surfaces of the acoustic fluid remain static during the calculation as discussed in Timperi (2009).

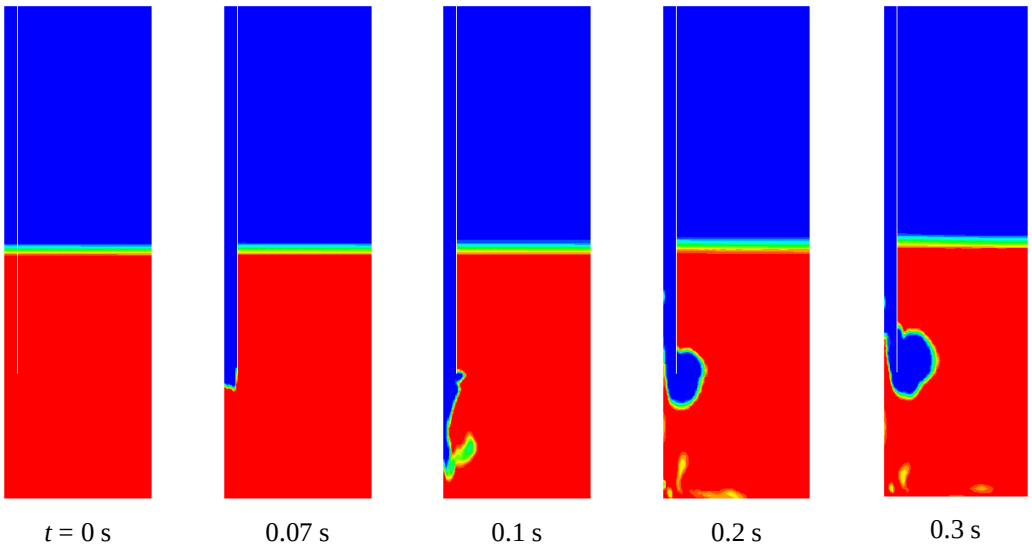

Figure 14. Volume fraction of water in a calculation with axisymmetric model.

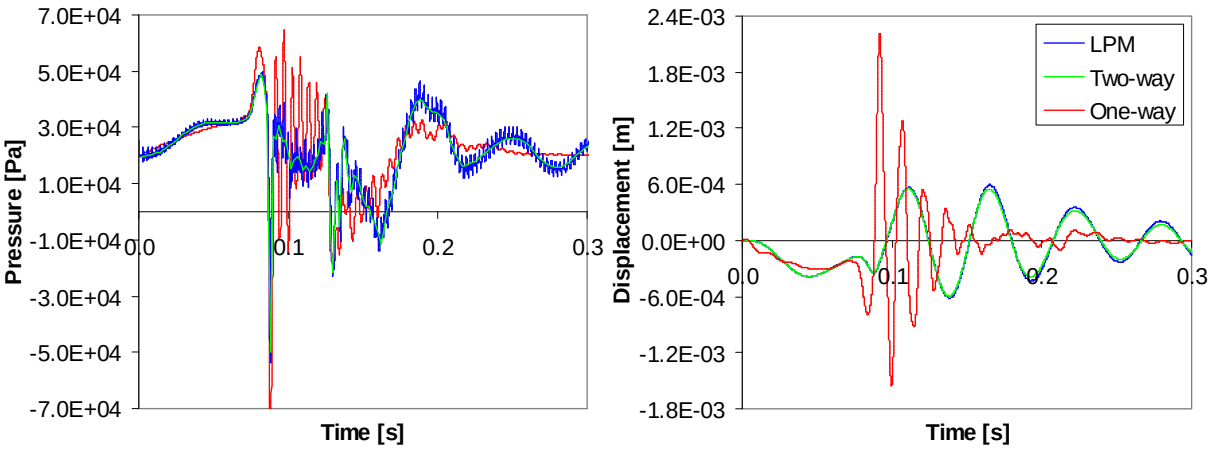

Figure 15. Wall pressure below pipe and wall displacement in calculations with axisymmetric model.

5.3 Comparison with PPOOLEX experiment

Numerical models used for the calculations are presented in Fig. 13. The CFD mesh had about 135 000 hexahedral cells. For the structure, a fairly detailed finite-element model consisting mainly of about 15 000 4-noded shell elements was used. Flexibility of disc springs and base structures under the four vertical support columns were modeled with linear springs. The VOF and k-ε models were used in the CFD calculation. Air was treated as ideal gas and a

logarithmic equation of state was used for water. Mass flow of air at the drywell inlet was set to a constant value of 805 g/s.

These calculations are the same as in Pättikangas et al. (2009) except for some modifications. Firstly, flexibility of the disc springs was adjusted to better fit the measured data. Secondly, a constant mass flow of air was used instead of the measured mass flow curve. The second modification was made because in Pättikangas et al. (2009) charging of the drywell with air was found to be significantly slower in the calculation compared to the experiment which is probably caused by delay in the mass flow sensor (Puustinen, 2008). As discussed below, the charging is still too slow in the calculation. One possible source for this difference is that also the measured maximum flow rate of 805 g/s is lower than in reality due to the slow response of the sensor.

Formation of the first bubble in the pool is shown in Fig. 16 for the calculation and experiment. Pressures and vertical displacements at the pool bottom are compared in Fig. 17. Charging of the drywell with air is still somewhat slower in the calculation, viz. the first bubble appears at the pipe outlet at t = 1.9 s and t = 1.5 s in the calculation and experiment, respectively. Therefore, in the figures times between the calculation and experiment have been synchronized to the moment when the first bubble appears. It is seen that the calculation with LPM shows qualitatively correct results. The wall pressure can be in this case separated into the components described in Timperi (2009): pressure caused by the blowdown and by wall motion. The calculation with rigid walls shows only the blowdown load, i.e. the effect of wall motion is not included. Amplitude and frequency of the pool motion obtained with LPM are fairly close to the experiment. The motion is mainly due to vertical oscillation of the whole pool and its frequency is about 12 Hz. The frequency is about 1.5 times higher in the one-way coupled calculation due to the absence of water. The smaller displacements obtained with one-way coupling may be caused by the higher eigenfrequency of the empty pool. In addition, damping of the pool motion is faster when the mass of water is neglected.

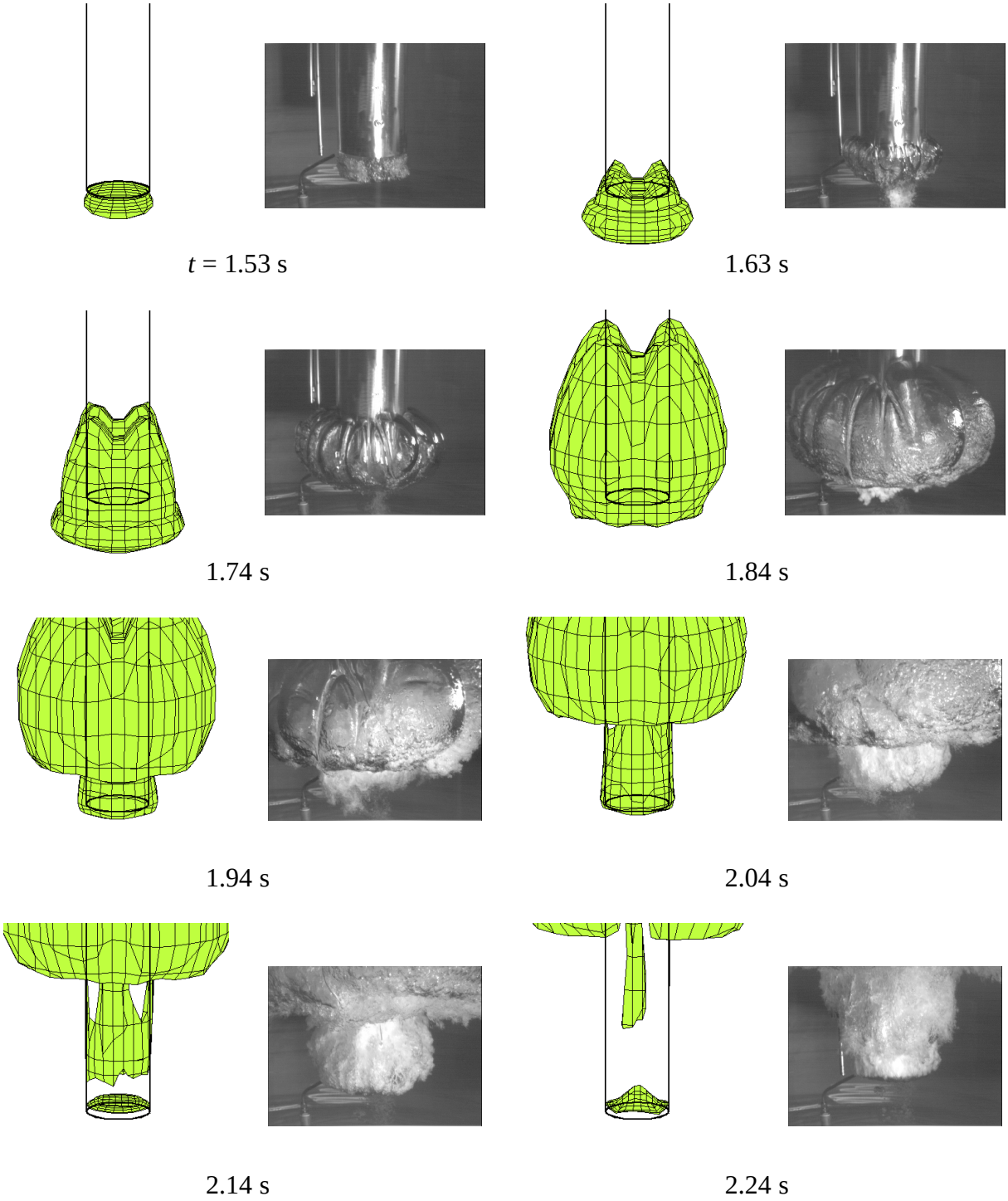

Figure 16. Formation of air bubble at the vent outlet in the PPOOLEX experiment and in the calculation.

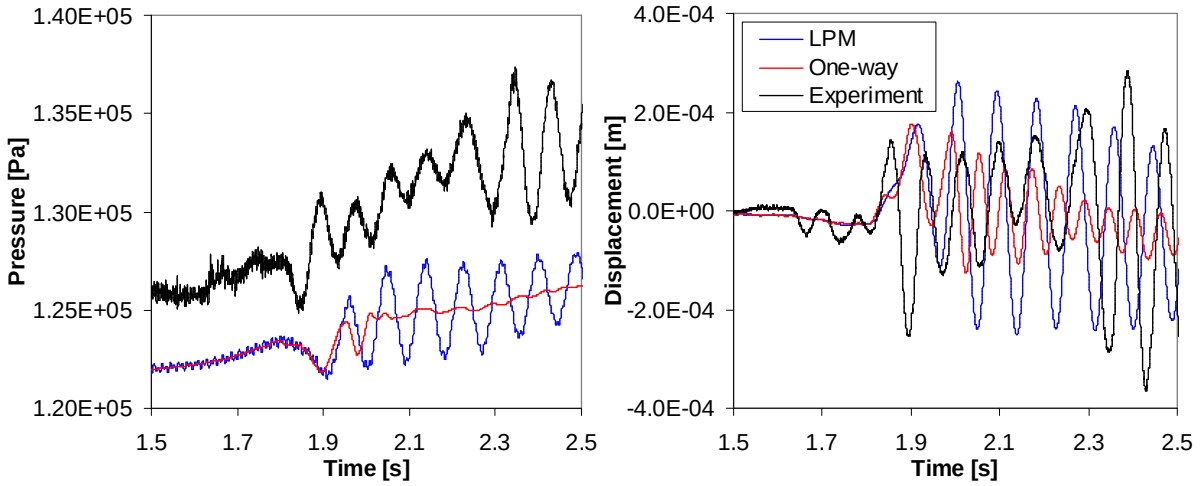

Figure 17. Wall pressure below pipe and wall displacement in the PPOOLEX experiment and in the calculations.

5.4 Modeling of realistic BWR containment

The numerical models representing a sector of the Olkiluoto 1 and 2 containments are shown in Figs. 18 - 20. One sixteenth, i.e. 22.5°, of the containment was modeled so that the sector includes one of the sixteen blowdown pipes. Symmetry boundary conditions were applied at the sides. Note that in reality the pipes are not distributed exactly evenly around the circumference, although even distribution was assumed here.

The CFD model had about 170 000 and 610 000 cells with the coarse and fine mesh, respectively. Only part of the drywell was modeled because a pressure boundary condition was used. The boundary condition represents the drywell pressurization in case of a full break of the main steam line and is shown in Fig. 21. The VOF model was used for the free surface and the k-ε model for modelling turbulence. The ideal gas law and a logarithmic equation of state suitable for compressible liquid were assumed for nitrogen and water, respectively. Time step was 0.5 ms.

The FEM model had about 5000 elements. Water in the wetwell was included in the structural model as an acoustic fluid because FSI was modeled with LPM. Also the upper water volumes of the containment were included as acoustic fluid. The bottom of the model was fully fixed.

For concrete, material properties E = 39 GPa, ν = 0.17 and ρ = 2400 kg/m^3 were used for elastic modulus, Poisson's ratio and density, respectively. For the steel cover above the reactor pressure vessel, values E = 206 GPa, ν = 0.3 and ρ = 7850 kg/m^3 were used. For water, values K = 2.224 GPa and ρ = 1000 kg/m^3 were used for bulk modulus and density, respectively.

The damping ratio was set to 5 % and 4 % for the concrete and steel, respectively (Regulatory Guide 1.61, 2007). The Rayleigh damping was used and these damping ratios were adjusted to be exact for frequencies 10 Hz and 150 Hz, which cover the frequency range of interest in this work.

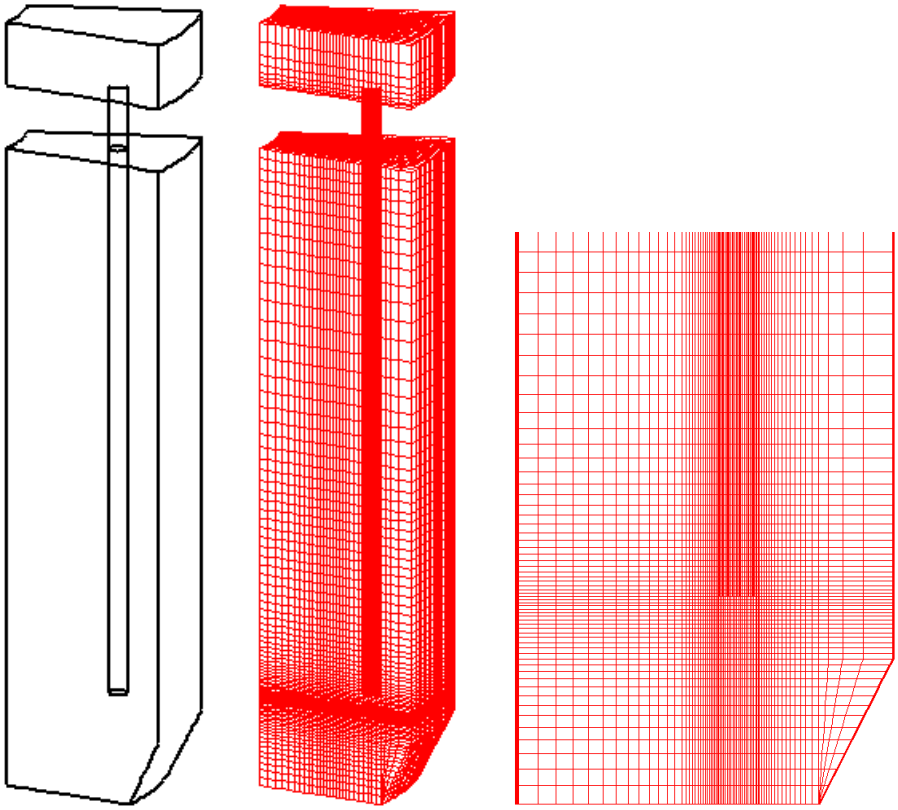

Figure 18. CFD geometry and mesh of the BWR containment.

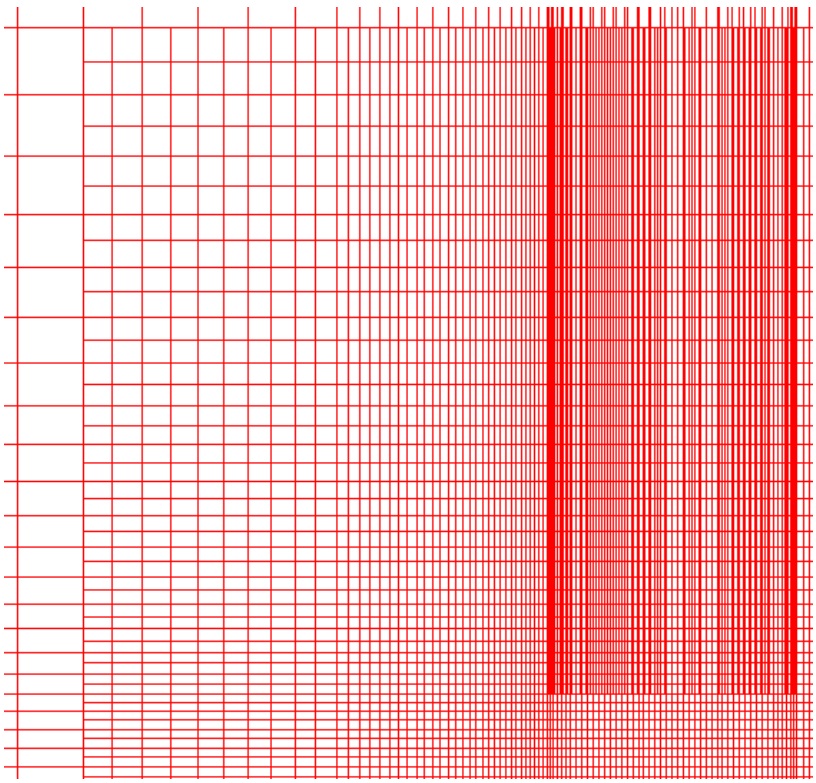

Figure 19. Refined mesh of the BWR containment near pipe outlet.

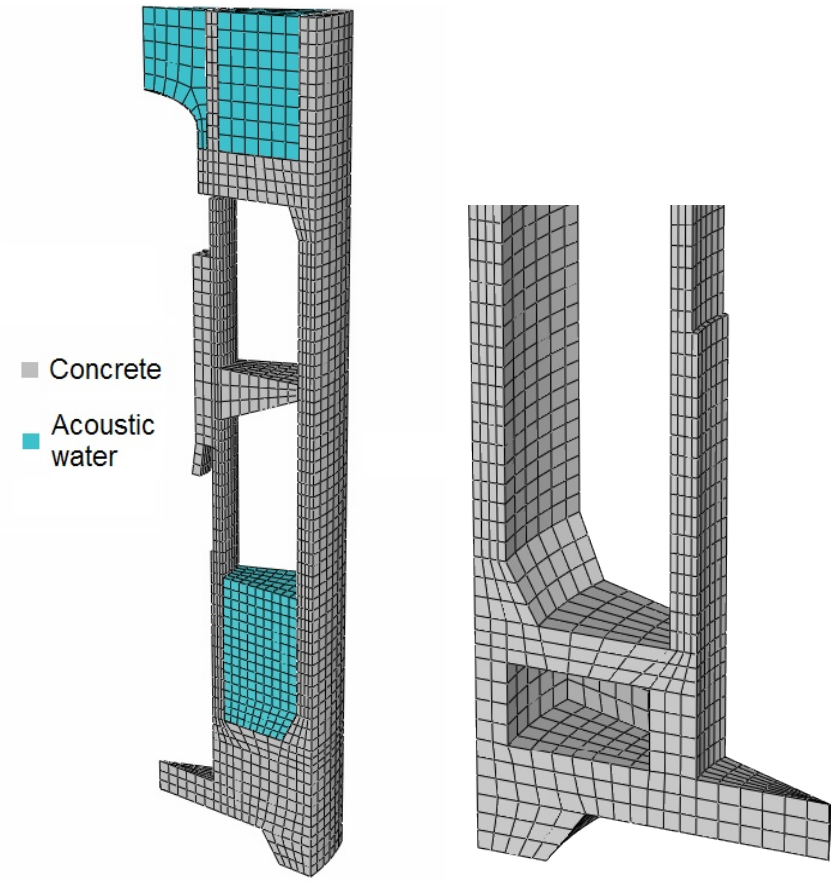

Figure 20. FEM mesh of the BWR containment.

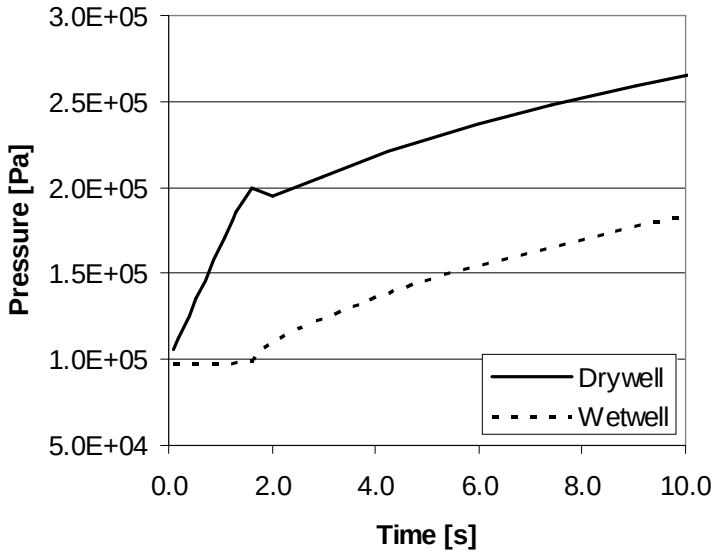

Figure 21. Gas pressure in the BWR drywell and wetwell in the early phase of steam line break. The drywell pressure is used as a boundary condition in the CFD model.

Fig. 22 shows the volume fraction of water in the BWR pool. The deformations and stresses of the concrete structures are shown in Fig. 23. The deformations are mainly due to the quasi-static pressurization of the containment, i.e. vibrations caused by the bubble formation and detachment are fairly small. The analysis duration was only 3 s, because it is unclear at which moment will the steam condensation start to affect the results.

Pressures are plotted as a function of time in Figs. 25 - 27. The shape of the pressure curve is quite similar to the ones obtained for the PPOOLEX facility. Note, however, that here the pressure oscillations after the water plug hit are not caused by the wall motion but by some fluid-dynamic mode, most probably due to water and/or gas compressibility. Note also that the pressure on the pool bottom is not taken directly below the pipe, where the peak pressure is largest.

Displacements of the containment are plotted as a function of time in Figs. 28 - 34. The displacement output locations are shown in Fig. 24. It is seen that the displacements are small, especially relative to the size of the containment. This is partly explained by the cylindrical shape of the containment, i.e. the hoop stresses in the walls support effectively. Another explanation for the small displacements is the concrete structure where the walls need to be thick, resulting in a rigid structure. Note that here we assumed a fully symmetric case, i.e. synchronous bubble formation and symmetry boundary conditions for the structure. An asymmetric case would most probably result in higher displacements, although a fully asymmetric bubble formation sounds a bit unrealistic for the initial blowdown phase. Another consequence of the structural symmetry boundary condition is that the lower frequency bending modes of the containment are suppressed.

The frequency of the structural motion is on the order of 20…30 Hz. This is clearly higher than that of the pressure load. A more rapid pressure pulse, such a as that induced by a condensing steam bubble, would probably cause larger structural effects, in particular for a resonance situation.

Fig. 35 compares shape of the bubble at t = 2.4 s in the one- and two-way coupled calculations. The differences between the calculations are surprisingly large when considering the very small structural deformations. The maximum displacement is only about 0.1 mm and the maximum wall velocity is only of order 1 mm/s. Another two-way calculation was performed where the structure was made artificially stiff and heavy so that even smaller deformations resulted; in this case the bubble shape and the pressure curves corresponded quite well with the one-way case. This indicates that the difference is not due to different numerical solution methods with and without moving mesh. However, the difference may still be of numerical rather than physical origin. Agreement between the moving and non-moving mesh calculations was good in Sec. 5.2, although the displacements were much larger. In Sec. 5.2, the time step size was short and the “sound wave Courant number” ($c\Delta t/\Delta x$) was about 2. In the BWR calculations, it is of order 15 which is clearly too large for accurate description of the pressure waves. Another difference is that in Sec. 5.2 the gas was assumed incompressible.

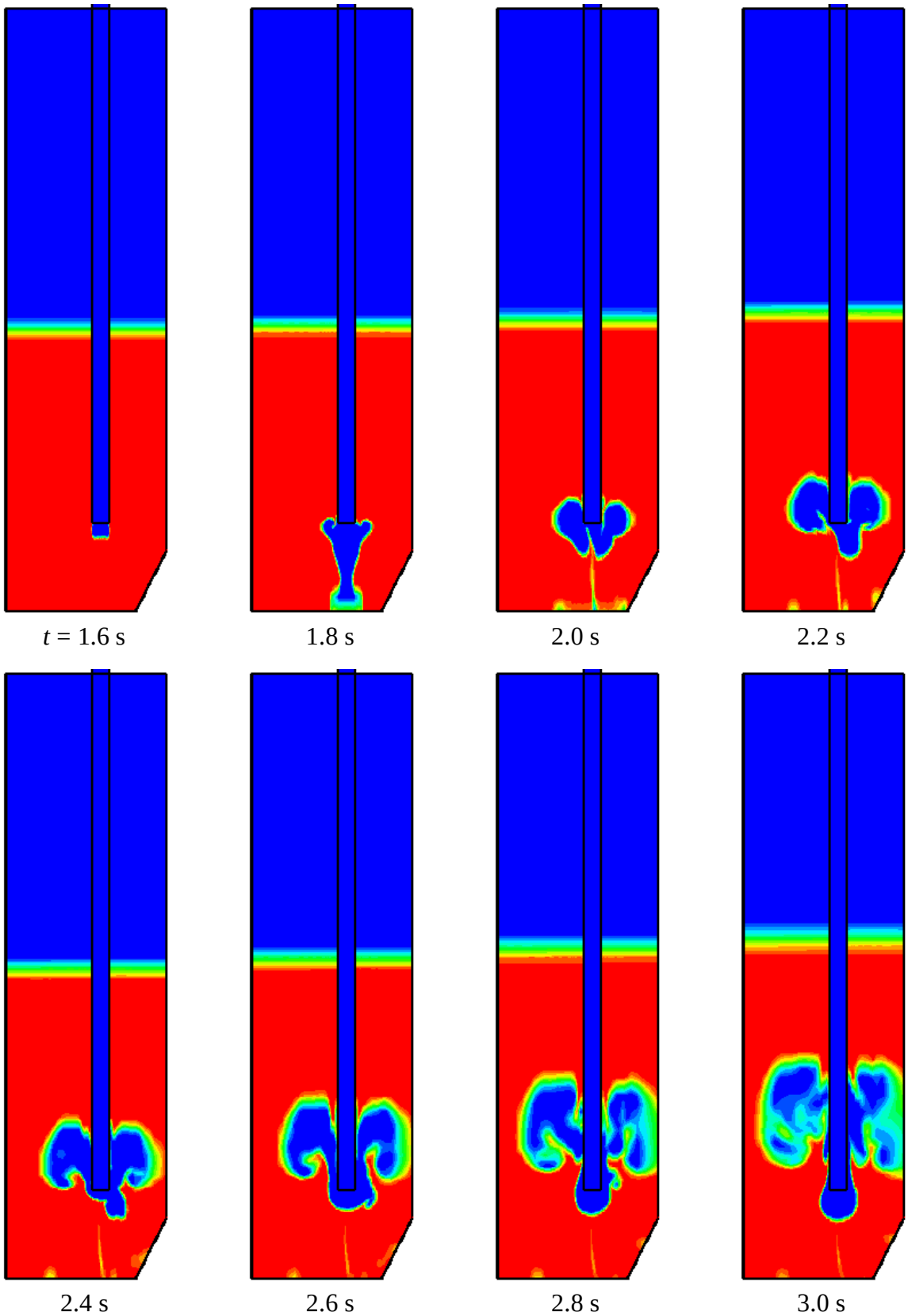

Figure 22. Volume fraction of water for a calculation of BWR containment.

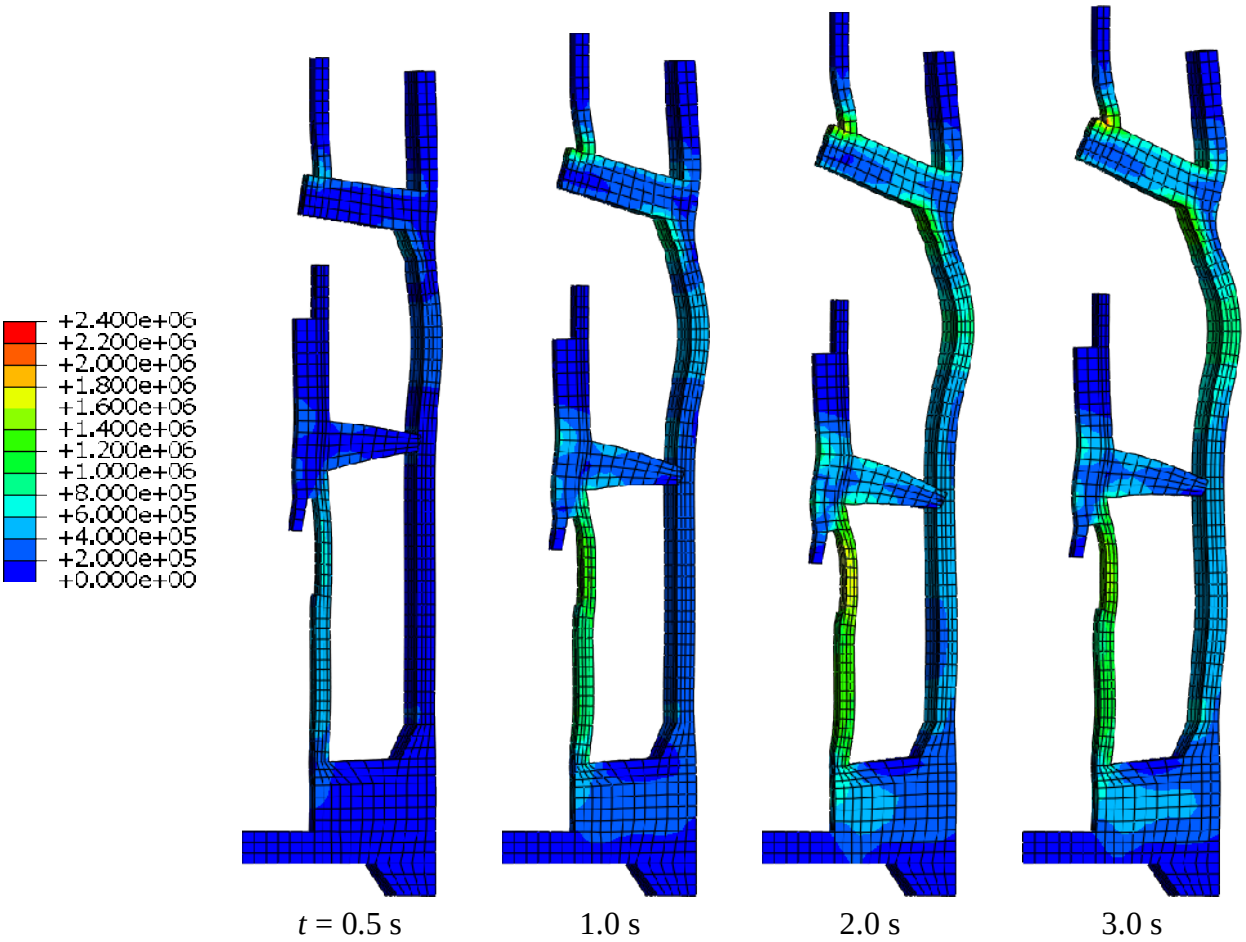

Figure 23. Von Mises stress (Pa) and deformation of the BWR containment. Note that effects of hydrostatic fluid pressure or structural gravity load are not included. The deformation scale factor is 5000.

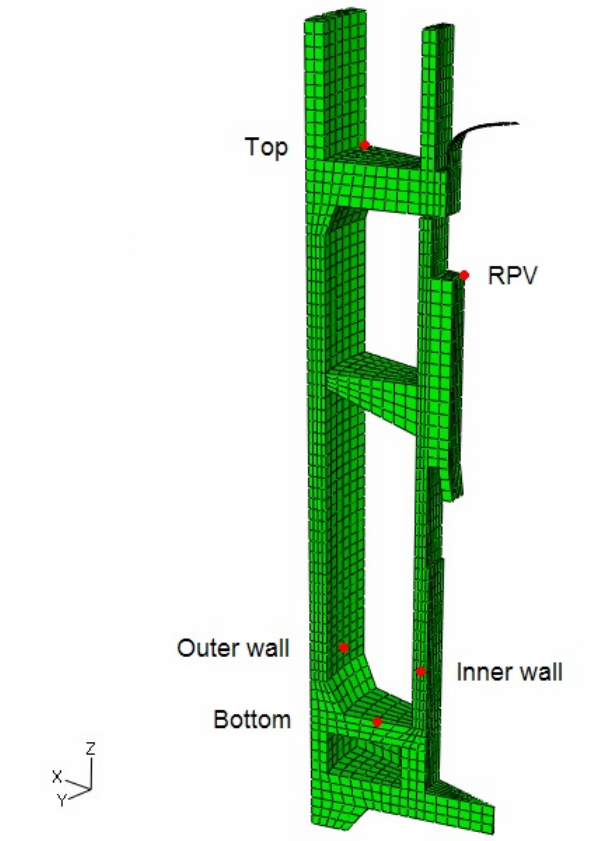

Figure 24. Locations of displacement output for the structural model.

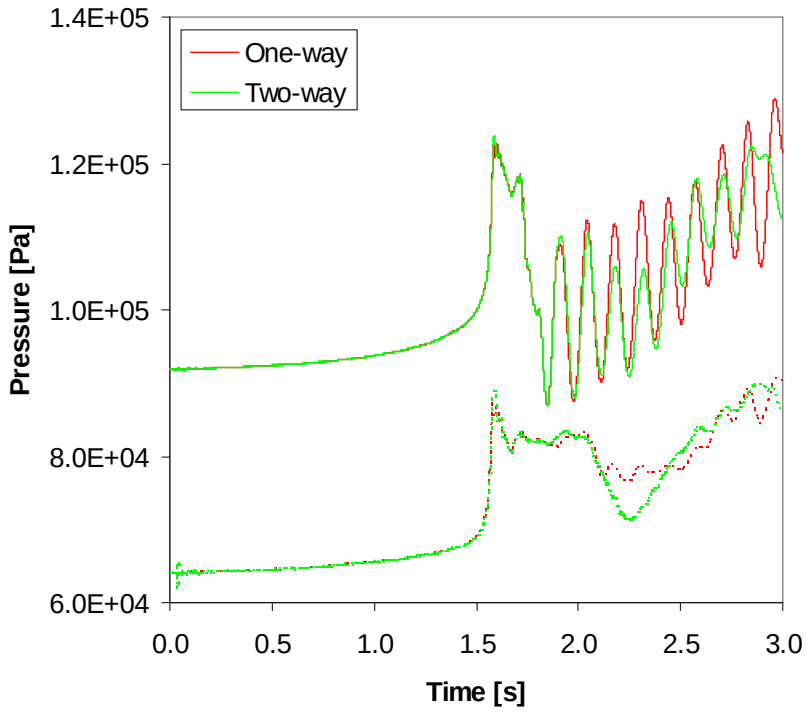

Figure 25. Pressure in the middle of pool bottom (solid lines) and at the outer wall at pipe outlet level (dotted lines) with one- and two-way coupling.

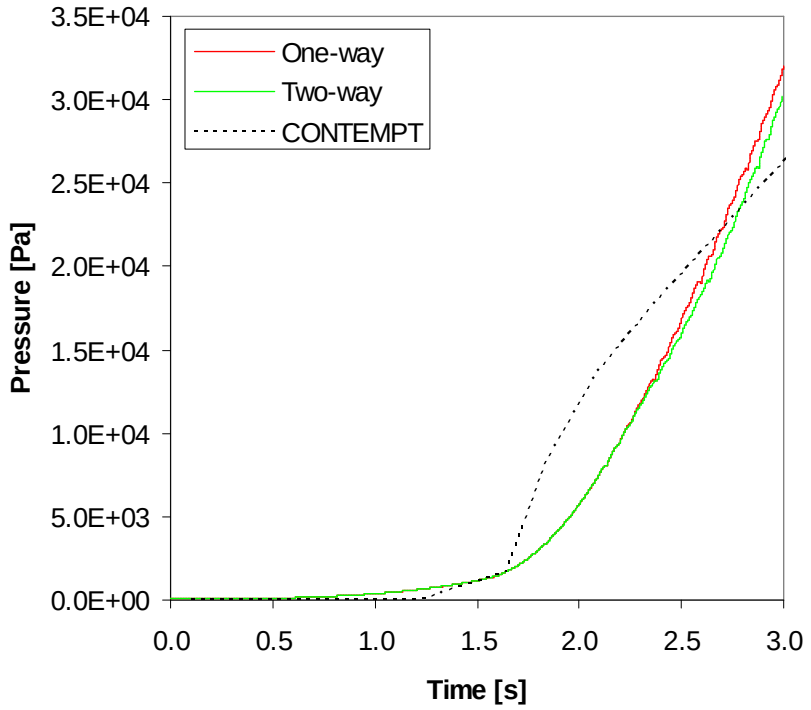

Figure 26. Pressure in the wetwell gas space with one- and two-way coupling and for CONTEMPT calculation.

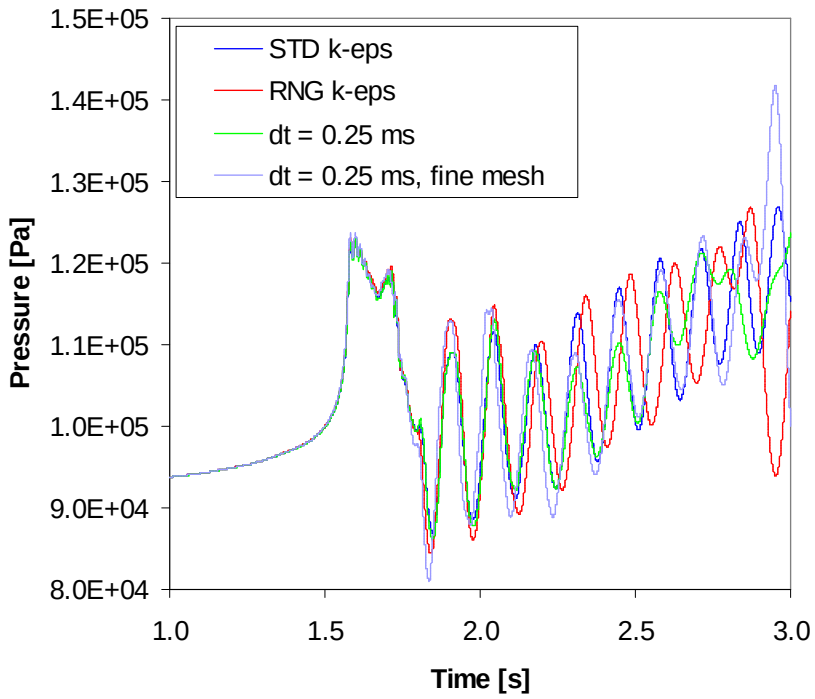

Figure 27. Pressure in the middle of pool bottom with one-way coupling by using different modeling settings.

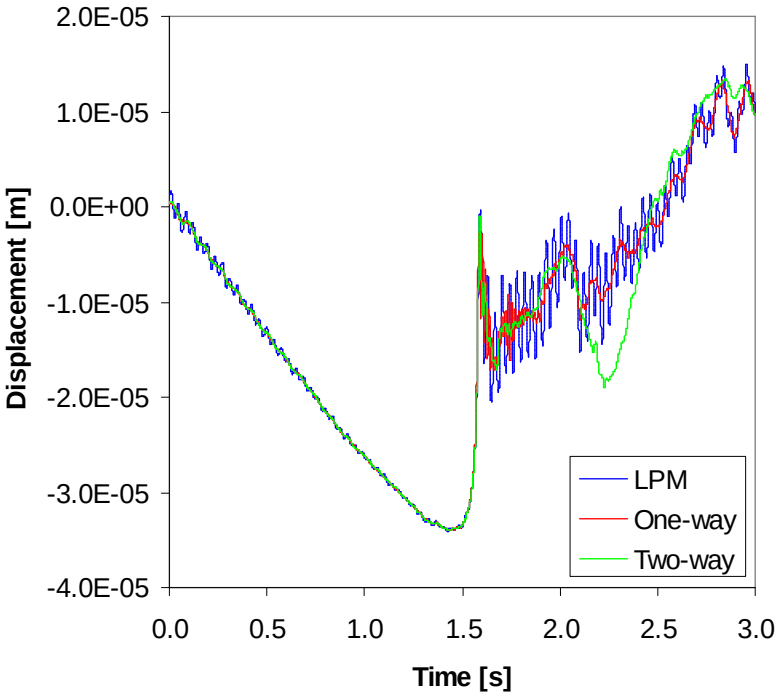

Figure 28. Radial displacement of location "Outer wall".

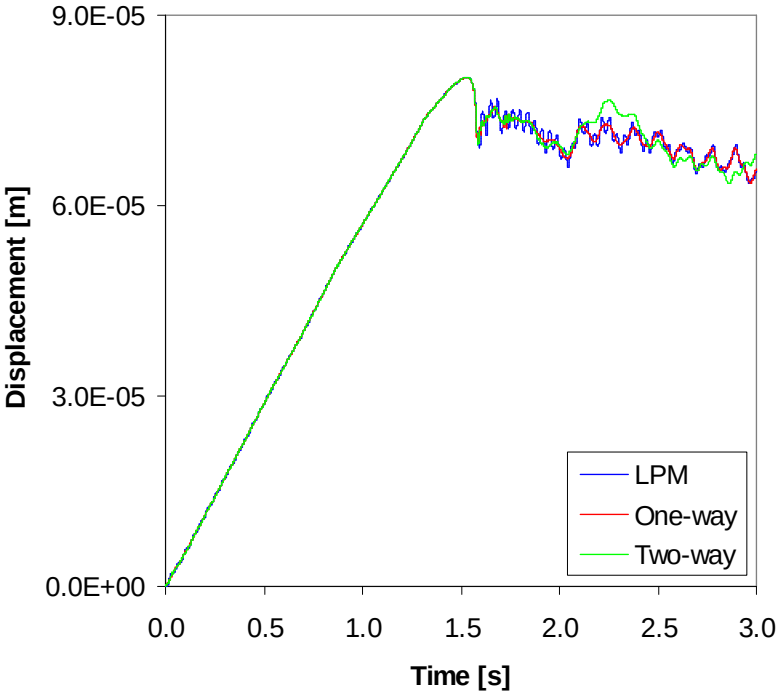

Figure 29. Radial displacement of location "Inner wall".

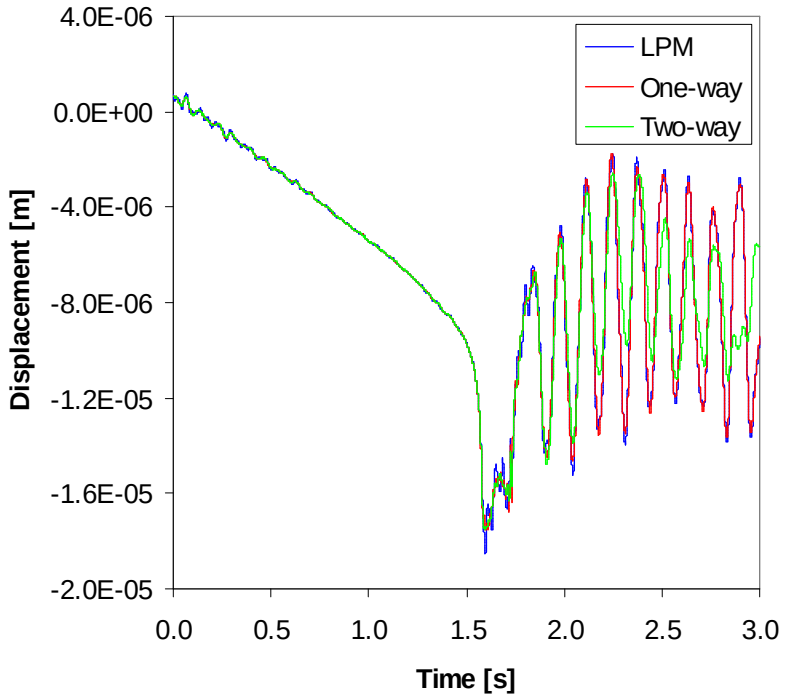

Figure 30. Vertical displacement of location "Bottom".

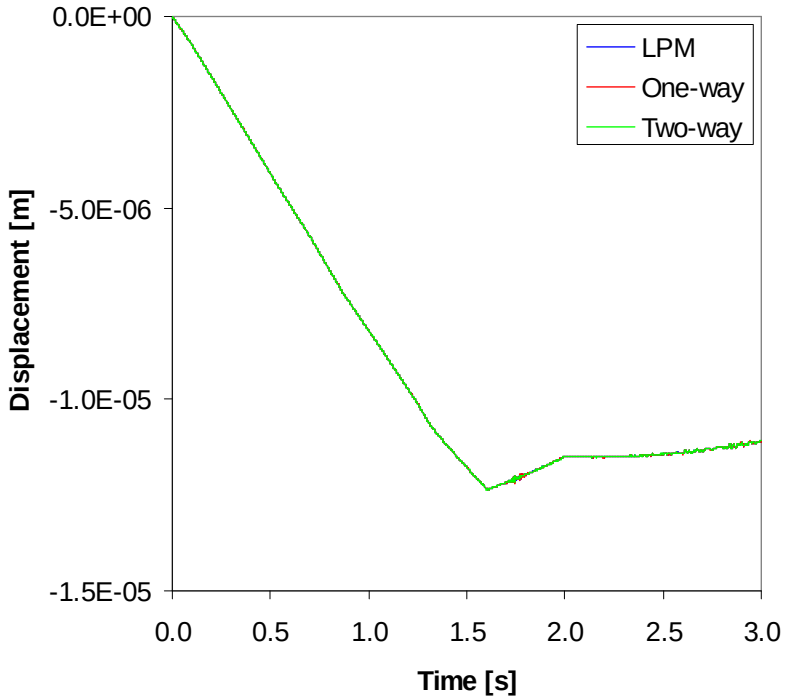

Figure 31. Radial displacement of location "RPV".

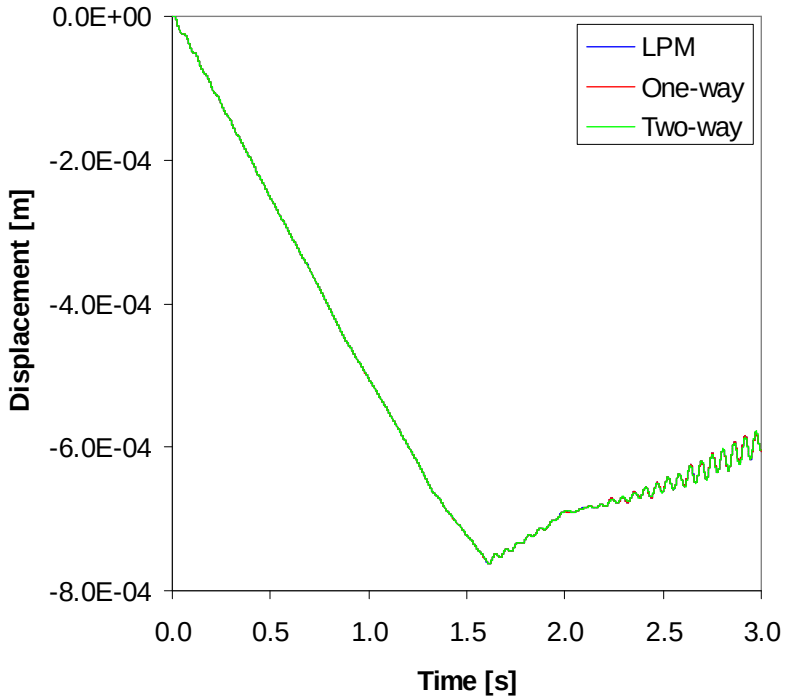

Figure 32. Vertical displacement of location "RPV".

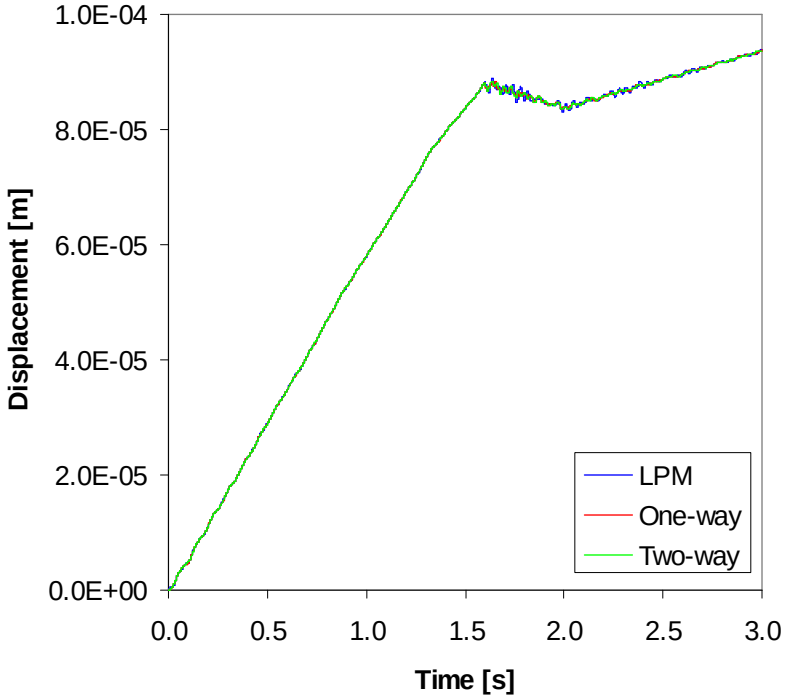

Figure 33. Radial displacement of location "Top".

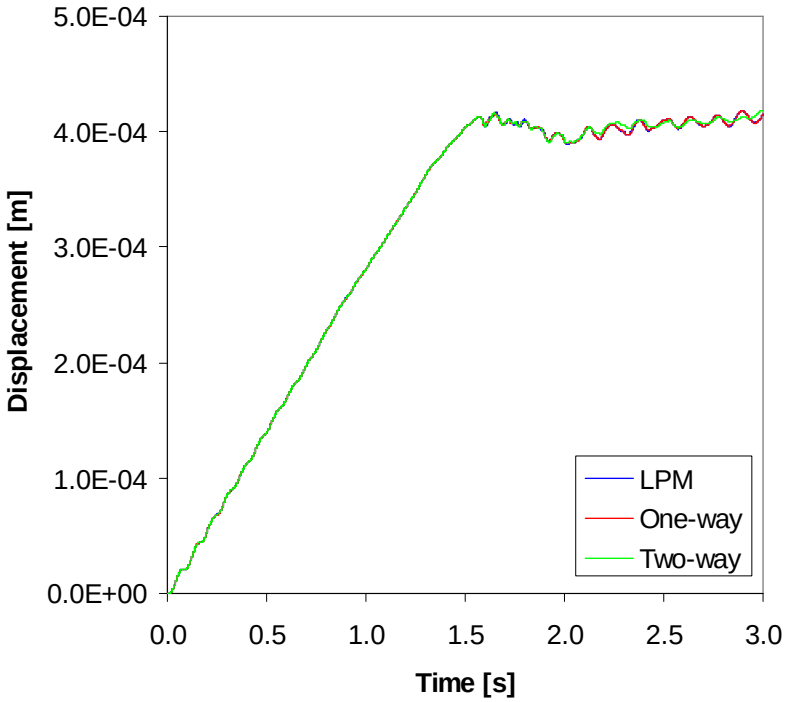

Figure 34. Vertical displacement of location "Top".

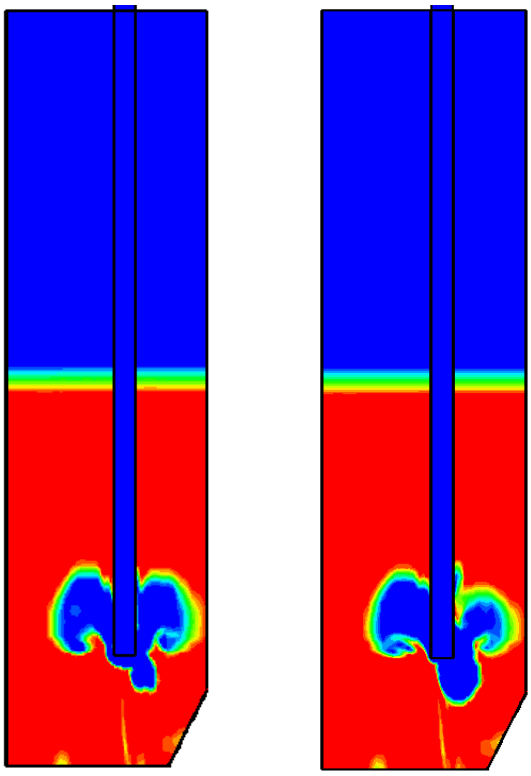

Figure 35. Comparison of bubble shape at t = 2.4 s obtained with one-way (left) and two-way (right) coupling.

6 Summary and conclusions

CFD and FEM modelling of has been performed for experiments performed with the PPOOLEX facility, which is a scaled-down model of a BWR pressure suppression containment. A model for wall condensation and a simple model for direct-contact condensation have been implemented in the commercial FLUENT code. The models have been tested against the PPOOLEX experiment WLL-05-02.

Comparison of the wall condensation model to the experiment was complicated by the uninsulated wall of the drywell of PPOOLEX. When the wall structures have been heated by the hot vapour, the wall condensation is determined by the heat transfer from the outer wall of the drywell to the ambient laboratory. In the CFD model, the chosen heat transfer coefficient on the outer wall determines the amount of condensation. In the calculation, this also affects to pressure level inside the drywell and wetwell.

In modelling the direct-contact condensation, the challenges are in the estimation of the interfacial surface area and the heat transfer coefficient. The heat transfer and condensation in the present calculation was found to be too weak. Some vapour was able to escape from the water pool to the gas space of the wetwell. An additional challenge is presented by modelling the interfacial drag in the different regions. In the drywell, some mist is formed by the bulk condensation. In the water pool, at the outlet of the vent pipe a large bubble is formed. In addition, small air bubbles are carried away by the flow in the water pool. More work is necessary to find suitable modelling techniques for these phenomena.

FSI calculations were presented by using a linear perturbation method which circumvents the numerical instability present in some cases with explicit two-way coupling. The method was first validated against a two-way coupled FSI calculation in a simplified blowdown case. Wall pressure and displacement obtained with LPM and with two-way coupling were in good agreement, whereas with one-way coupling the absence of the added mass effect was clearly seen. Validation was also performed against the PPOOLEX SLR-05-02 experiment where air was blown into the pool water. A reasonable agreement in wall pressure and displacement was found between the experiment and LPM calculation. Calculation with one-way coupling showed qualitatively incorrect results for the wall pressure. In addition, the structural displacements were smaller compared to the experiment and to those obtained with LPM. Because of the added mass effects, using only one-way FSI coupling is not necessarily conservative in condensation pool simulations.

Preliminary FSI calculations of the non-condensable initial phase of LOCA in a BWR containment were also carried out. Effect of FSI was quite small due to the relatively stiff and heavy pool structures. The FSI calculations gave only slightly larger displacements than one-way pressure mapping. Stresses and displacements due to the wetwell blowdown load were fairly small and the largest structural effects were caused by quasi-static pressurization of the containment. A symmetric case (simultaneous bubble formation for all pipes) was assumed; fully anti-symmetric case would give higher loads but may be unrealistic for the initial phase. A partial explanation for the low structural response is the low frequency of the blowdown load compared to the eigenfrequency of the system. Water hammers due to rapidly condensing steam bubbles could cause considerably larger deformations, in particular for a resonance situation. In addition, FSI should have a larger effect for more rapid pressure transients.

References

Cook, R., Malkus, D., Plesha, M. and Witt, R., 2002. Concepts and applications of finite element analysis. Wiley & Sons, Inc.

Huber, P.W., Kalumuck, K.M. and Sonin, A.A., 1979. Fluid-structure interactions in containment systems: small-scale experiments and their analysis via a perturbation method. 1st International Seminar on Fluid-Structure Interaction in LWR Systems, held in conjunction with the 5th International Conference on Structural Mechanics in Reactor Technology, Berlin, Germany, August 13 - 17, 1979.

Lahey, R. T. and Moody, F. J., 1993. The thermal hydraulics of a boiling water nuclear reactor. 2nd Edition, American Nuclear Society.

Laine, J. and Puustinen, M., 2009. PPOOLEX experiments on wall condensation. Research report, Lappeenranta University of Technology, Nuclear Safety Research Unit, CONDEX 3/2008, 34 p.

Puustinen, M., 2008. Personal communication.

Pättikangas, T., Niemi, J. and Timperi, A., 2009. Modelling of blowdown of steam in the pressurized PPOOLEX facility. VTT Technical Research Centre of Finland, Research Report VTT-R-03073-09, Espoo, Finland, 52 p.

Regulatory Guide 1.61, 2007. Damping values for seismic design of nuclear power plants. U.S. Nuclear Regulatory Commission.

Sonin, A.A. 1980. Rationale for a linear perturbation method for the flow field induced by fluid-structure interactions. Journal of Applied Mechanics, Vol. 47, P. 725-728.

Timperi, A. 2009. Fluid-structure interaction calculations using a linear perturbation method. 20th International Conference on Structural Mechanics in Reactor Technology, Espoo, Finland, August 9 - 14, 2009.

Title	CFD and FEM modeling of PPOOLEX experiments
Author(s)	Timo Pättikangas, Jarto Niemi and Antti Timperi
Affiliation(s)	VTT Technical Research Centre of Finland
ISBN	978-87-7893-308-9
Date	January 2011
Project	NKS-R / POOL
No. of pages	39
No. of tables	2
No. of illustrations	35
No. of references	9

Abstract

Large-break LOCA experiment performed with the PPOOLEX experimental facility is analysed with CFD calculations. Simulation of the first 100 seconds of the experiment is performed by using the Euler-Euler two-phase model of FLUENT 6.3. In wall condensation, the condensing water forms a film layer on the wall surface, which is modelled by mass transfer from the gas phase to the liquid water phase in the near-wall grid cell. The direct-contact condensation in the wetwell is modelled with simple correlations. The wall condensation and direct-contact condensation models are implemented with user-defined functions in FLUENT.

Fluid-Structure Interaction (FSI) calculations of the PPOOLEX experiments and of a realistic BWR containment are also presented. Two-way coupled FSI calculations of the experiments have been numerically unstable with explicit coupling. A linear perturbation method is therefore used for preventing the numerical instability. The method is first validated against numerical data and against the PPOOLEX experiments. Preliminary FSI calculations are then performed for a realistic BWR containment by modeling a sector of the containment and one blowdown pipe. For the BWR containment, one- and two-way coupled calculations as well as calculations with LPM are carried out.

Key words Large-break LOCA, Condensation pool, pressure suppression pool, BWR, CFD, fluid-structure interactions, FSI

Available on request from the NKS Secretariat, P.O.Box 49, DK-4000 Roskilde, Denmark.
Phone (+45) 4677 4045, fax (+45) 4677 4046, e-mail nks@nks.org, www.nks.org